Copy 1 of 2

MECHANICAL PROPERTIES OF MULTI-YEAR SEA ICE, PHASE II

Progress Report 2

April 1983

by

G.F.N. Cox, J.A. Richter, W.F. Weeks and M. Mellor

U.S. Army Cold Regions Research and Engineering Laboratory
Hanover, NH 03755

Prepared for

Shell Development Company

Minerals Management Service

INTRODUCTION

This progress report presents the results of the constant strain-rate triaxial tests which were performed during the months of January and February, 1983.

TRIAXIAL TESTS

Conventional triaxial tests were performed on the closed-loop testing machine using sample preparation and testing techniques similar to those employed in Phase I. As a result of our experience in Phase I, the triaxial cell was modified to increase its load bearing capacity to 350 kN (80,000 lbs) and confining pressure capacity to 24 MPa (3500 lbf/in.^{2}). Heavier latex membranes were also placed around the sample to prevent penetration of hydraulic fluid into the sample. A 22 kN (100,000 lb) load cell was provided by Shell to measure axial forces in excess of 11 kN (50,000 lb). The upper cylinder was also modified such that tests could be performed at confining pressure/axial stress ratios of 0.25 and 0.50.

A total of 55 triaxial tests were performed on multi-year pressure ridge samples at different test temperatures, strain-rates, and confining pressures. The number of tests at each test condition is summarized in Table 1. In Phase I, triaxial tests were performed on multi-year floe samples at axial stress/confining pressure ratios of 0.46 and 0.64 at the same temperatures and strain-rates.

Triaxial Strength

A detailed tabulation of the results from the triaxial tests is given in Appendix A. The average confined compresive strength of the ice, σ_1, for each test condition is plotted against the confining pressure ($\sigma_2=\sigma_3$) at faialure in Figure 1. Average uniaxial compressive strength data from

Table 1: Number of triaxial tests at different temperatures, strain-rates and axial stress/confining pressure ratios (σ_r/σ_a).

$\dot{\varepsilon}$ / T	$\sigma_r/\sigma_a = 0.25$		$\sigma_r/\sigma_a = 0.05$		
	10^{-5}/s	10^{-3}/s	10^{-5}/s	10^{-3}/s	
-5°C (23°F)	10V		9V	9V	28V
-20°C (-4°F)		9V	9V	9V	27V
	10V	9V	18V	18V	55V

V = Vertical

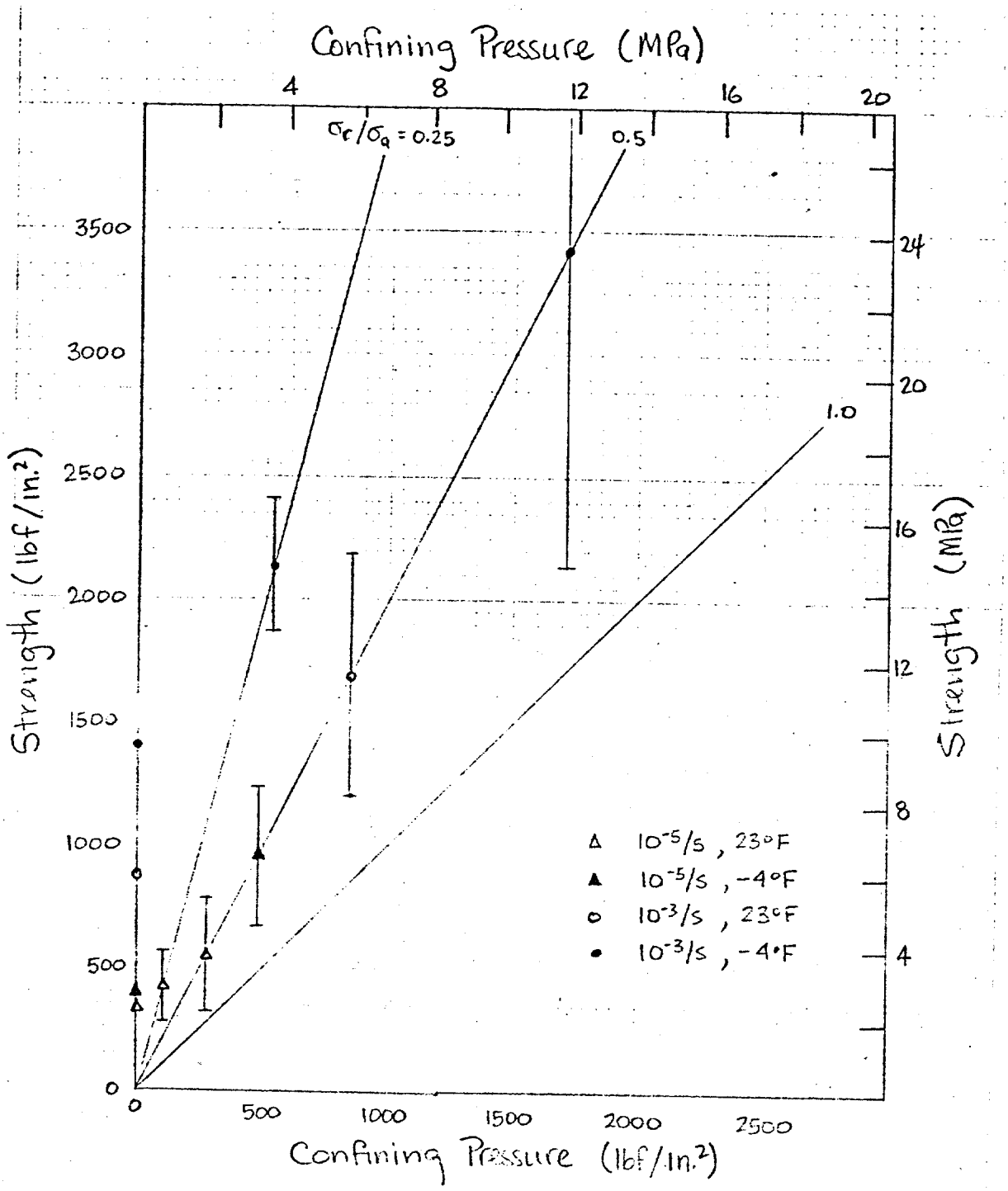

Figure 1: Compressive strength versus confining pressure for multi-year pressure ridge samples at different temperatures and strain-rates. The bars denote one standard deviation from the mean.

Phase I is included for comparison. In making comparisons between the unconfined and confined compressive strength data, it should be noted that the Phase I ridge samples had a much lower porosity. Table 2 summarizes the Phase II triaxial strength data.

As observed in Phase I, the confined compressive strength increases with decreasing temperature, increasing strain-rate, and increasing confining pressure. Due to variability of the ice structure between samples, the data show considerable scatter. The data at 10^{-5}/s suggests that failure of the ridge ice samples at low strain-rates may be described by a Tresca or Von Mises yield criteria. The yield surface paralles the hydrostat ($\sigma_r/\sigma_a = 1.0$). This supports the observations made by Jones who investigated the confined compressive strength of fresh water polycrystalline ice at low strain-rates.

The Phase II final report will also include a discussion on the initial tangent modulus data from the triaxial tests and examine the variation of the triaxial strength and modulus data with sample porosity.

Table 2. Summary of triaxial strength data.

	Triaxial Strength							
	Maximum		Minimum		Mean		Mean Porosity	
	(MPa)	(lbf/in.^{2})	(MPa)	(lbf/in.^{2})	(MPa)	(lbf/in.^{2})	(ppt)	Samples
-5°C (23°F)								
10^{-5}/s V, 0.25	3.95	573	1.14	166	2.86±0.98	415±142	79	10
10^{-5}/s V, 0.50	6.61	959	2.28	330	3.81±1.59	552±231	86	9
10^{-3}/s V, 0.50	17.94	2602	5.43	788	11.70±3.41	1697±495	78	9
-20°C (-4°F)								
10^{-3}/s V, 0.25	17.07	2475	11.58	1679	14.77±1.90	2141±275	77	9
10^{-5}/s V, 0.50	11.03	1600	3.95	573	6.59±1.97	956±286	82	9
10^{-3}/s V, 0.50	38.63	5602	8.34	1210	23.50±8.73	3408±1266	57	9

APPENDIX A

Triaxial Test Data

This appendix contains the results from the constant strain-rate triaxial tests (TRI). The parameters listed for each test are defined in the Index. As no displacement transducers were placed directly on the sample, the initial tangent modulus data given in Column 8 is based on the full sample strain. TRI-3-5/.5 denotes those tests conducted at a strain-rate of 10^{-3}/s, a temperature of -5°C, and a confining pressure/axial stress ratio of 0.5.

INDEX

Column No.	Symbol	Description
1	σ_m, psi	Peak Stress
2	ε_m(GL),%	Strain at σ_m determined by the DCDT's over a guage length of 5.5 inches
3	ε_m(FS),%	Strain at σ_m determined by the extensometer over the full sample length of 10 inches
4	t_m, sec	Time to peak stress
5	σ_e, psi	Stress at end of test
6	ε_e(FS),%	Full sample strain at end of test
7	t_e, sec	Time to end of test
8	E_i(GL),x10^6psi	Initial tangent modulus determined using strains found over the gauge length
9	E_o(GL),x10^6psi	Secant modulus determined using gauge length strains
10	E_o(FS),x10^6psi	Secant modulus determined using full sample strains
11	S_i,°/oo	Sample salinity at test temperature
12	ρ, lb/ft^3	Sample density at test temperature
13	V_b,°/oo	Brine volume at test temperature
14	V_a,°/oo	Air volume at test temperature
15	n,°/oo	Porosity at test temperature
16	σ_e /σ_m	Ratio of end to peak stress
17	Ice squareness, in	Sample squareness after ends are milled
18	End cap squareness, in	Sample squareness after endcaps are mounted
19	Shim, in	Amount of shim stock inserted between low end of sample and actuator before testing
20	ν_o	Initial Poisson's Ratio; circumferential and gauge length strain measurements used
21	ν_m	Poisson's ratio at peak stress; ε_m(C) and ε_m(GL) used
22	ε_m(C),%	Strain at σ_m determined by the circumferential extensometer

Also Note: FILE B-3-5 indicates Below Level Ice

10^{-3}/sec Strain Rate

-5°C Test Temperature

FILE TRI-5-5/.25

SAMPLE # 01	02	03	04	05	06	07	08	09	10	11	12	13	14	15	16	17	18	19	20	21	22
RA208-134/161 460	0.940	930.0	360	5.00	5000				0.049	0.03	51.12	0.3	107.6	107.9	0.783	0.009	0.000	0.000			
RA208-166/193 427	0.790	750.0	310	5.00	5000	0.707			0.054	0.04	52.77	0.4	78.9	79.3	0.726	0.004	0.003	0.004			
RA208-198/225 366	0.920	940.0	326	5.00	5000	0.168			0.040	0.16	51.22	1.4	106.1	107.5	0.891	0.009	0.007	0.008			
RA208-259/280 515	0.580	590.0	334	5.00	5000	0.408			0.089	0.80	52.65	7.3	82.1	89.4	0.649	0.003	0.006	0.006			
RB212-077/104 166	0.360	342.0	165	5.00	5000	0.217			0.046	1.24	54.60	11.7	48.9	60.6	0.994	0.004	0.004	0.004			
RB212-163/190 555	1.000	999.0	377	5.00	5000	0.309			0.056	0.12	53.34	1.1	69.1	70.2	0.679	0.008	0.002	0.002			
RB212-194/221 549	1.000	999.0	376	5.00	5000	0.245			0.055	0.33	53.75	3.1	62.3	65.3	0.685	0.009	0.009	0.010			
RB213-066/093 286	0.450	444.0	230	5.00	5000	0.179			0.064	1.03	54.05	9.6	58.1	67.7	0.804	0.009	0.016	0.016			
RB213-097/124 253	0.390	390.0	201	5.00	5000	0.194			0.065	1.21	53.73	11.2	64.0	75.2	0.794	0.010	0.006	0.006			
RA208-290/317 573	0.790	820.0	402	5.00	5000	0.291			0.073	0.79	54.10	7.4	56.9	64.3	0.702	0.011	0.007	0.008			

FILE TRI-5-5/.5

SAMPLE # 01	02	03	04	05	06	07	08	09	10	11	12	13	14	15	16	17	18	19	20	21	22
RA210-236/263 330	5.000	5000					0.172			0.09	47.23	0.7	175.6	176.3		0.010	0.008	0.008			
RA210-459/486 446	2.810	2810	442	5.00	5000	0.267			0.016	0.29	51.48	2.6	101.7	104.3	0.991	0.004	0.010	0.010			
RA210-536/563 895	0.960	960.0	641	5.00	5000	0.297			0.093	0.51	55.76	4.9	27.4	32.3	0.716	0.010	0.010	0.010			
RB213-255/282 362	0.650	660.0	350	5.00	5000	0.212			0.056	2.22	55.12	21.1	41.2	62.3	0.967	0.004	0.004	0.004			
RB216-230/257 489	0.730	730.0	430	5.00	5000	0.209			0.067	1.43	53.11	13.1	75.1	88.2	0.879	0.005	0.004	0.004			
RB216-330/357 350	0.910	910.0	330	5.00	5000	0.362			0.038	1.15	54.69	10.8	47.2	58.0	0.943	0.006	0.006	0.006			
RB217-367/394 577	0.900	910.0	525	5.00	5000	0.287			0.064	1.31	56.42	11.0	16.9	27.9	0.910	0.011	0.009	0.010			
RB217-443/470 959	0.520	540.0	625	5.00	5000	0.436			0.184	1.04	56.62	10.1	15.0	25.2	0.652	0.034	0.014	0.014			
RA210-372/399 557	1.320	1340	485	5.00	5000	0.339			0.042	0.09	45.66	0.7	203.1	203.8	0.871	0.006	0.006	0.006			

FILE TRI-3-5/.5

SAMPLE # 01	02	03	04	05	06	07	08	09	10	11	12	13	14	15	16	17	18	19	20	21	22
RA210-490/517 1830	0.590	5.80	1369	5.00	50.00	0.574			0.310	0.32	53.58	3.0	65.2	68.2	0.748	0.004	0.006	0.006			
RA211-233/260 1544	0.440	4.20	979	5.00	50.00	0.461			0.351	0.04	52.34	0.4	86.4	86.7	0.534	0.007	0.016	0.016			
RB213-286/313 1870	0.410	4.00	1432	5.00	50.00	0.650			0.456	1.34	55.14	12.7	39.5	52.2	0.766	0.010	0.003	0.004			
RB216-124/151 1926	0.520	4.70	979	5.00	50.00	0.685			0.370	1.50	53.32	13.8	71.5	85.3	0.508	0.007	0.010	0.010			
RB216-262/289 1294	0.350	3.10	1019	5.00	50.00	0.526			0.370	0.95	51.61	8.5	100.4	108.9	0.554	0.012	0.013	0.014			
RB217-236/263 1838	0.420	3.90	1424	5.00	50.00	0.601			0.438	0.40	53.13	3.7	73.2	76.8	0.775	0.005	0.006	0.006			
RB217-267/294 1584	0.600	5.60	1424	5.00	50.00	0.531			0.264	0.95	55.13	9.0	39.0	48.1	0.899	0.019	0.008	0.008			
RB217-399/426 2602	1.010	10.60	1806	5.00	50.00	0.715			0.258	0.62	56.51	6.0	14.5	20.6	0.694	0.016	0.005	0.006			
RA210-059/086 788	0.280	2.80	788	5.00	50.00	0.419			0.281	0.02	48.38	0.2	155.5	155.7	1.000	0.025	0.004	0.004			

FILE TRI-3-20/.25

SAMPLE # 01	02	03	04	05	06	07	08	09	10	11	12	13	14	15	16	17	18	19	20	21	22
RA208-025/052 2125		0.610	6.00	1114	5.00	50.00	0.482		0.348	0.02	50.07	0.1	128.0	128.0	0.524	0.004	0.002	0.002			
RA208-340/367 2467		0.700	7.20	995	5.00	50.00	0.334		0.352	1.10	56.46	3.6	17.7	21.4	0.403	0.031	0.012	0.012			
RA211-078/105 1679		0.460	4.60	1679	0.46	4.60	0.428		0.365	0.02	50.95	0.1	112.6	112.7		0.006	0.002	0.002			
RA211-127/154 1822		0.470	4.80	740	5.00	50.00	0.470		0.388	0.03	49.36	0.1	140.3	140.4	0.406	0.010	0.004	0.004			
RB212-132/159 2475		0.650	6.40	1066	5.00	50.00	0.555		0.381	0.23	52.60	0.7	84.1	84.8	0.431	0.007	0.003	0.004			
RB212-326/353 2157		0.610	6.30	1027	5.00	50.00	0.297		0.354	1.28	54.89	4.1	45.2	49.3	0.476	0.006	0.004	0.004			
RB212-047/074 1974		0.610	6.10	788	5.00	50.00	0.546		0.324	0.81	53.36	2.5	71.4	73.9	0.399	0.003	0.006	0.006			
RB212-239/266 2236		0.580	5.70	931	5.00	50.00	0.589		$386.0	1.70	55.39	5.5	36.9	42.4	0.416	0.007	0.004	0.004			
RB213-156/183 2332		0.690	6.90	1027	5.00	50.00	0.536		0.338	1.58	55.48	5.1	35.3	40.4	0.440	0.007	0.005	0.006			

FILE TRI-5-20/.5

SAMPLE # 01	02	03	04	05	06	07	08	09	10	11	12	13	14	15	16	17	18	19	20	21	22
RA210-90/117 740	5.000	5000					0.303			0.03	50.33	0.1	123.4	123.5		0.004	0.007	0.008			
RA210-133/160 851	1.520	1530	851	5.00	5000	0.479		0.056		0.03	50.94	0.1	112.8	112.9	1.000	0.000	0.005	0.006			
RA211-266/293 1039	0.700	710.0	772	5.00	5000	0.297		0.148		0.04	51.92	0.1	95.8	95.9	0.743	0.007	0.006	0.006			
RB216-156/183 573	5.000	5000					0.282			1.96	50.55	5.8	121.3	127.1		0.005	0.010	0.010			
RB216-188/215 820	1.010	1030	820	5.00	5000	0.300		0.081		0.66	51.88	2.0	97.0	99.0	1.000	0.006	0.022	0.022			
RB216-361/388 971	0.780	750.0	812	5.00	5000	0.318		0.124		1.00	55.71	3.3	30.7	33.9	0.836	0.025	0.004	0.004			
RB216-432/459 1600	0.680	670.0	947	5.00	5000	0.452		0.235		1.47	56.53	4.9	16.9	21.7	0.592	0.015	0.010	0.010			
RB217-191/218 963	1.390	1380	939	5.00	5000	0.386		0.069		0.53	53.11	1.6	75.5	77.1	0.975	0.007	0.013	0.014			
RB217-335/362 1050	1.100	1110	955	5.00	5000	0.391		0.095		1.83	54.96	5.9	44.5	50.4	0.910	0.008	0.005	0.006			

FILE TRI-3-20/.5

SAMPLE # 01	02	03	04	05	06	07	08	09	10	11	12	13	14	15	16	17	18	19	20	21	22
RA210-194/221 2674	0.610	5.40	1942	5.00	50.00	0.830			0.438	0.02	51.77	0.1	98.4	98.4	0.700	0.002	0.004	0.004			
RA210-341/368 2578	0.790	7.80	1958	5.00	50.00	0.689			0.326	0.11	51.48	0.3	103.5	103.8	0.760	0.011	0.003	0.004			
RA210-567/594 4011	0.880	8.50	2196	5.00	50.00	1.021			0.456	0.83	56.43	2.7	18.0	20.7	0.547	0.007	0.003	0.004			
RB213-225/252 3008	0.680	6.60	1448	5.00	50.00	0.901			0.442	2.22	55.25	7.2	39.9	47.0	0.481	0.004	0.004	0.010			
RB213-342/369 4584	1.000	9.40	2992	5.00	50.00	0.936			0.458	1.65	55.60	5.4	33.2	38.6	0.653	0.004	0.004	0.004			
RB216-089/116 3374	0.490	4.50	3374	0.49	4.50	0.838			0.689	0.29	52.55	0.9	85.0	89.9		0.006	0.004	0.004			
RB216-392/419 3629	0.910	9.00	1974	5.00	50.00	0.860			0.399	1.78	56.22	5.8	22.6	28.4	0.544	0.007	0.010	0.010			
RB217-052/079 1210	0.210	2.00	1210	0.21	2.00	0.639			0.576	0.14	53.71	0.4	64.7	65.1		0.007	0.002	0.002			
RB218-363/390 5602	1.200	12.00	2929	5.00	50.00	1.000			0.467	0.55	56.60	1.8	14.8	16.6	0.523	0.005	0.005	0.006			

Copy 2 of 2

MECHANICAL PROPERTIES OF MULTI-YEAR SEA ICE, PHASE II

Progress Report 1

March 1983

by

G.F.N. Cox, J.A. Richter, W.F. Weeks and M. Mellor

U.S. Army Cold Regions Research and Engineering Laboratory

Hanover, NH 03755

Prepared for

Shell Development Company

Minerals Management Service

INTRODUCTION

This progress report describes the work performed in the Mechanical Properties of Multi-Year Sea Ice Program, Phase II, from 14 April 1982 to 31 January 1983. During this period, ice samples were obtained from several multi-year pressure ridges in the Beaufort Sea and shipped to CRREL for testing. Uniaxial compression tests were then performed on both horizontal and vertical samples to examine the effect of orientation on ice strength. We also completed the uniaxial tension and constant load compression tests described in the proposal. During the latter part of January we began working on the constant load tension and triaxial tests.

This progress report includes a detailed description of the field sampling program and presents the results from the constant strain-rate compression and tension tests. The next progress report will include the results from the triaxial tests.

FIELD SAMPLING PROGRAM

Our Phase I sampling program occurred between 3 and 15 April 1981. Although we had scheduled the Phase II sampling program for essentially the same time period in 1982, delays associated with establishing the funding level of the project kept the field operation from starting until 14 April 1982. Therefore, we were very concerned that a period of "warm" weather would cause us difficulties and that we would have to load the shipping boxes with dry ice while at the sampling sites. Fortunately this did not occur. Also we were favored with extremely good flying and working weather (limited ice fog and light winds). In fact the one day that ice fog curtailed flying we had not planned to work on the ice as a dry ice shipment

We finally selected a floe north of Leavitt Island where several floes were located near to each other and contained several well-rounded ridges that we estimated to be at least two summers old (Figure 1). The first sampling location (Ridge A) was on a thick multi-year floe with lateral dimensions of roughly 50 m. Although the ice had clearly been deformed, there was no cleanly delineated linear ridge. Therefore, we sited two of our sampling locations on high points and two sampling locations in swales. A sketch map showing the general topography of the sampling area is given in Figure 2. Figure 3 shows an oblique aerial photograph of the site (located in the foreground). The small building (which was transported to the site by helicopter) provides a sense of scale. The location of Hole 10 (see Figure 2) is indicated by an arrow in Figure 3). Figure 4 shows a surface view of the floe. The 1 to 1.5 m freeboard is evident. A total of 11 holes were taken at this site for a total core length of 48.70 m. The ice at this site was generally characterized by a high volume of included air as compared with the ridges that we had sampled in 1981. Therefore, we decided to sample several other ridges in the near vicinity to see if they also contained such large amounts of included gas or perhaps would prove to be similar to the ridges we sampled previously.

These additional ridges were found on two floes located approximately 200 m to the north of our first sampling site. The second ridge (Ridge B) was approximately 27 m long and was located on the smallest of these two floes (Figure 5). It is possible that these two floes were initially part of the same larger floe, which had been split. The ice proved to be quite solid

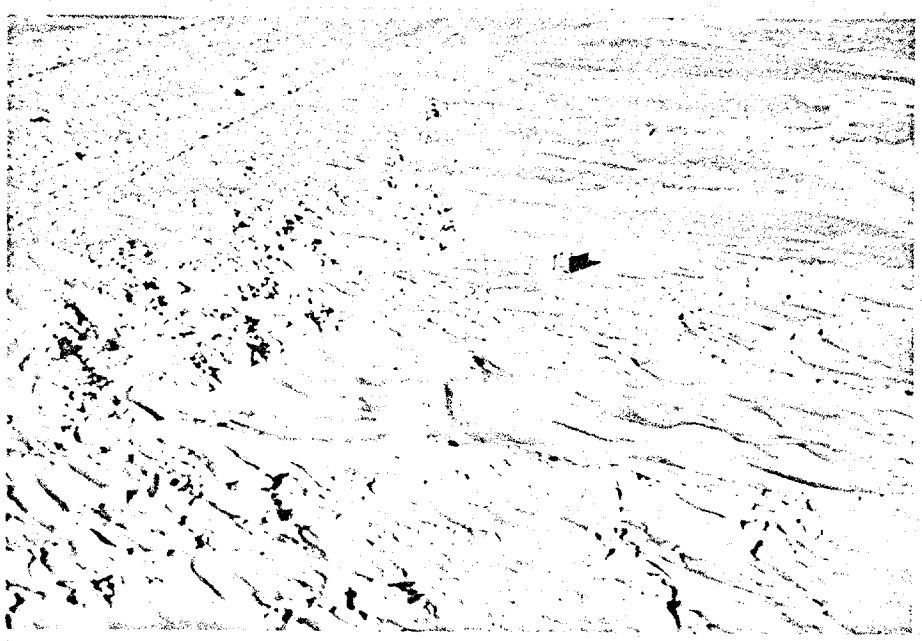

Figure 1: Aerial view of multi-year floe, designated as Ridge A, where first 11 cores were obtained.

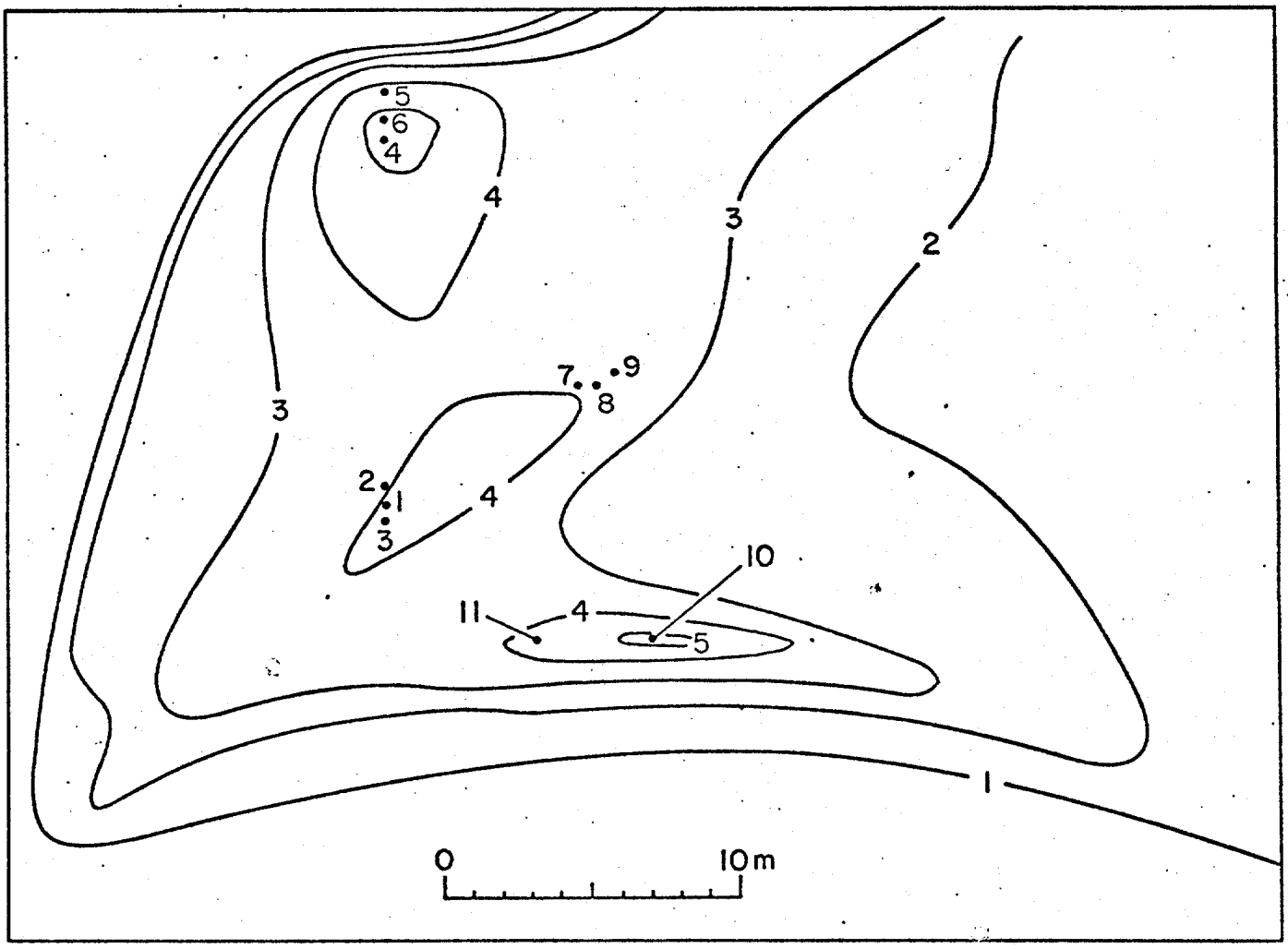

Figure 2: Sketch map of multi-year floe, Ridge A, showing location of the ice sampling sites.

Figure 3: Oblique aerial view of Ridge A sampling site.

Figure 4: Surface view of Ridge A sampling site.

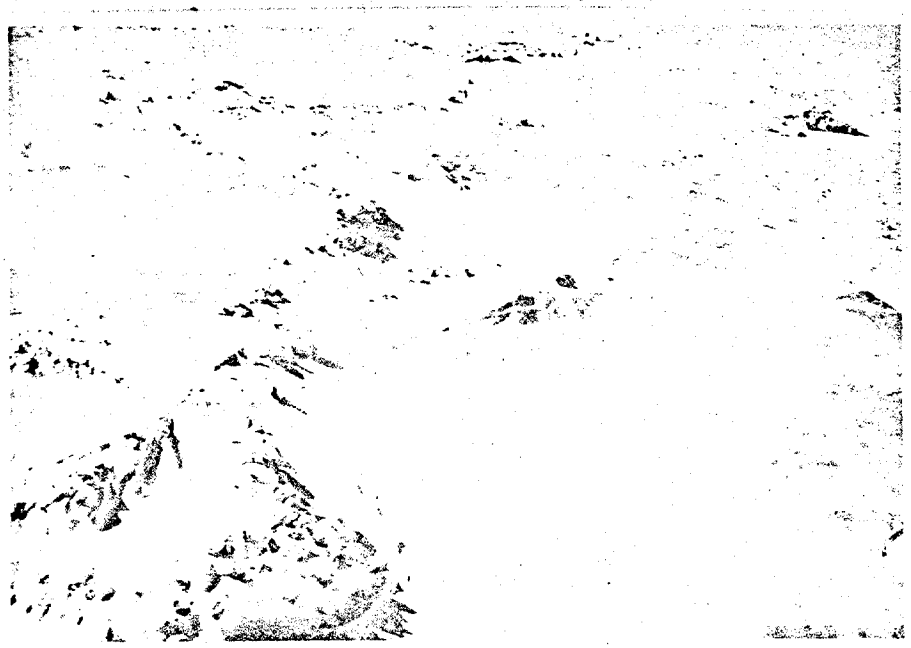

Figure 5: Aerial view of sampling area containing Ridges B, C, and D.

and massive with significantly less included gas. A sketch of a profile of this ridge showing the location of specific core sites is given in Figure 6. Note the sharp vertical termination of the ridge on the "right-hand" edge of the floe. The length of core obtained from this ridge was 50.32 m.

The third ridge sampled was approximately 75 m long and was the largest ridge on the adjoining floe. A profile of this ridge (Ridge C) is given in Figure 7. Figure 5 shows an aerial view of this ridge (marked as C) as well as of Ridges B and D. Ridge C, although broad, was quite clearly defined. Figure 8 shows coring underway on this ridge. A total of 67.11 m of core were obtained from this ridge for use as test specimens. A 9.53 m core was also obtained (penetrating completely through the floe) to use in petrographic studies. In addition all the 12 in. diameter core was obtained from this ridge.

The last ridge sampled was roughly parallel to Ridge C. Ridge D can also be seen in Figures 5. This ridge was 53.6 m in length and also was clearly delineated. Figure 9 shows the split end of the ridge where its blocky deformed structure could be examined. The total core recovery from Ridge D was 47.93 m.

In addition, 3.83 m of core were obtained from a floe which appeared to contain undeformed multi-year ice. Figure 10 shows an aerial view of the site. A judgment of the adequacy of this selection will await petrographic examination of the core.

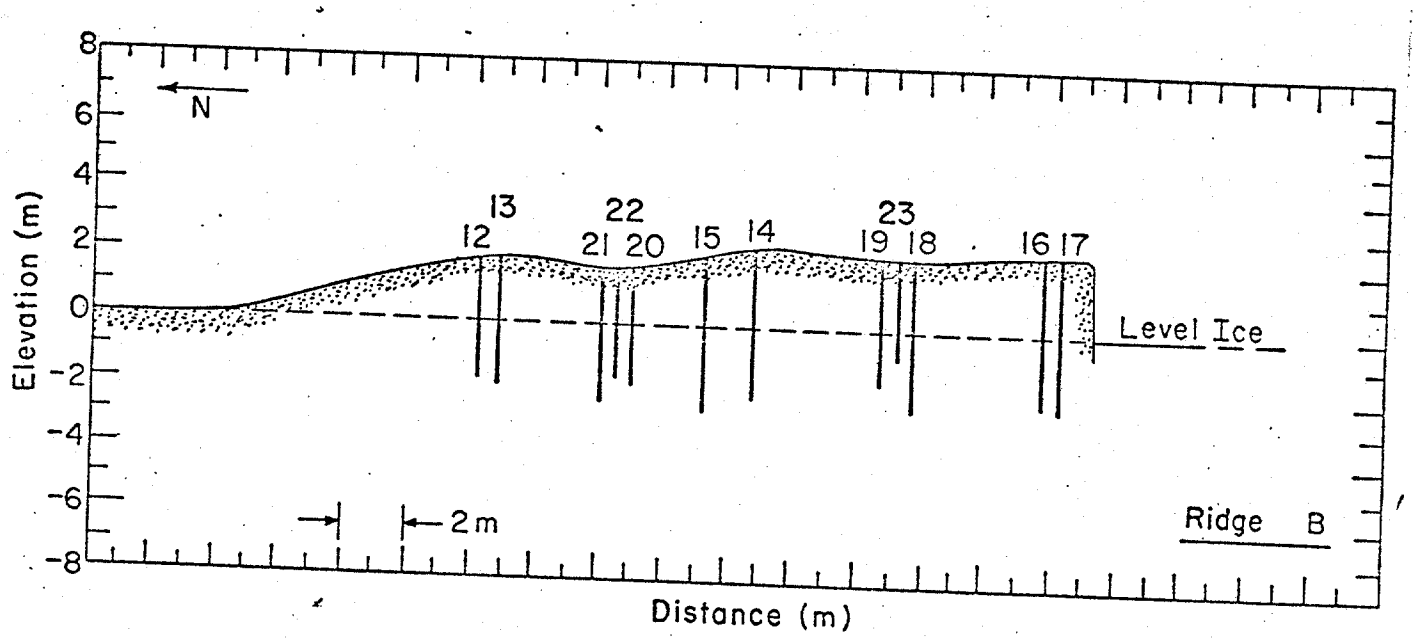

Figure 6: Sketch of Ridge B profile showing the location of the ice sampling sites.

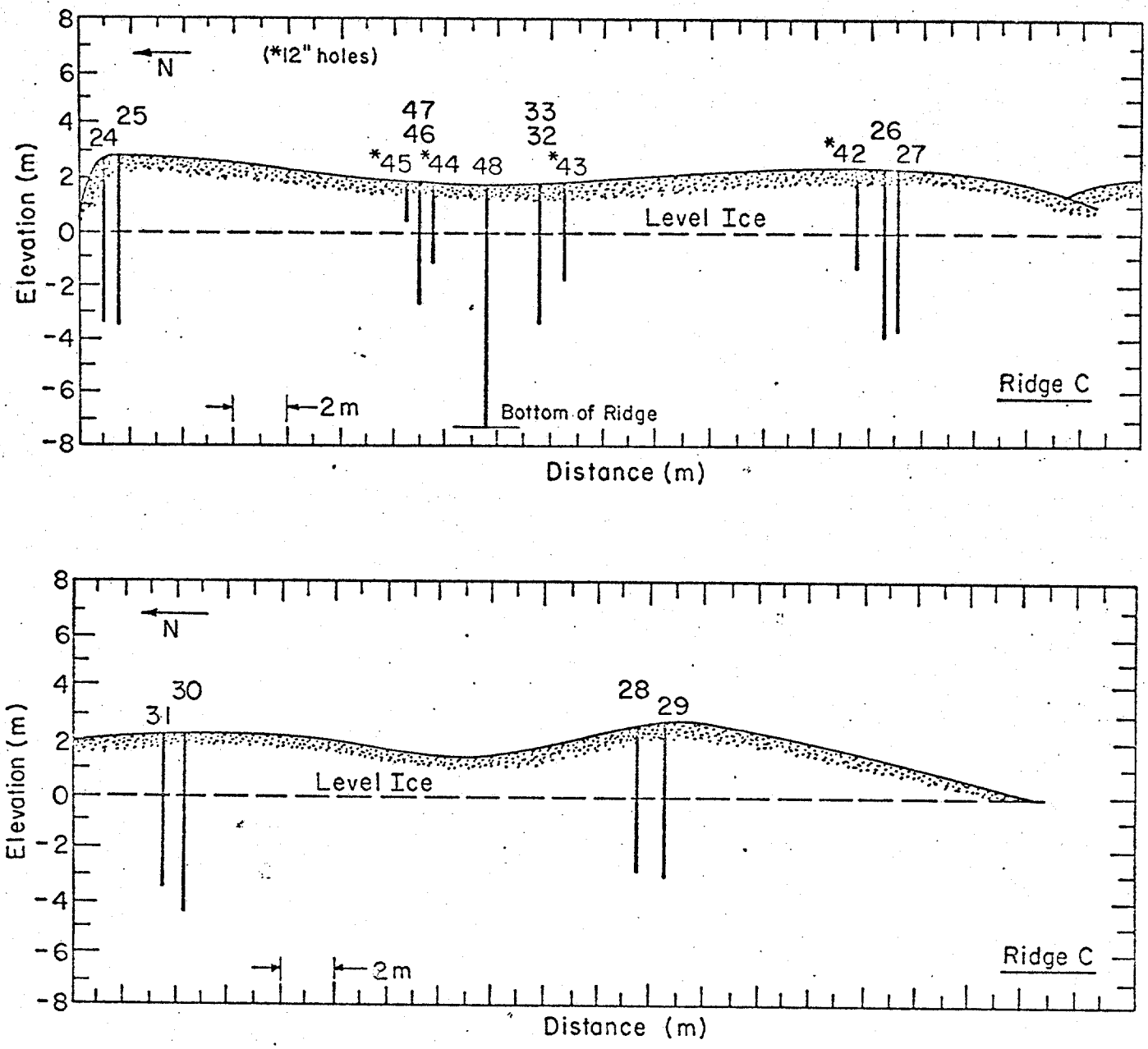

Figure 7: Sketch of Ridge C profile showing the location of the ice sampling sites.

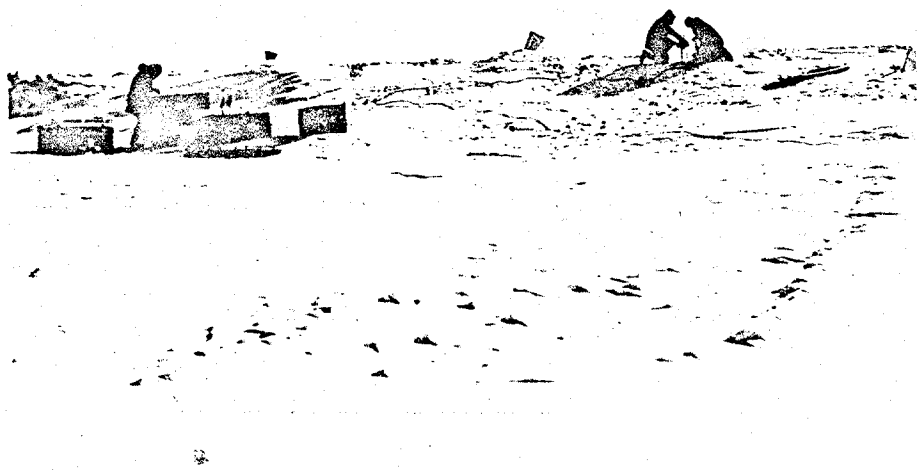

Figure 8: Coring operation on Ridge C.

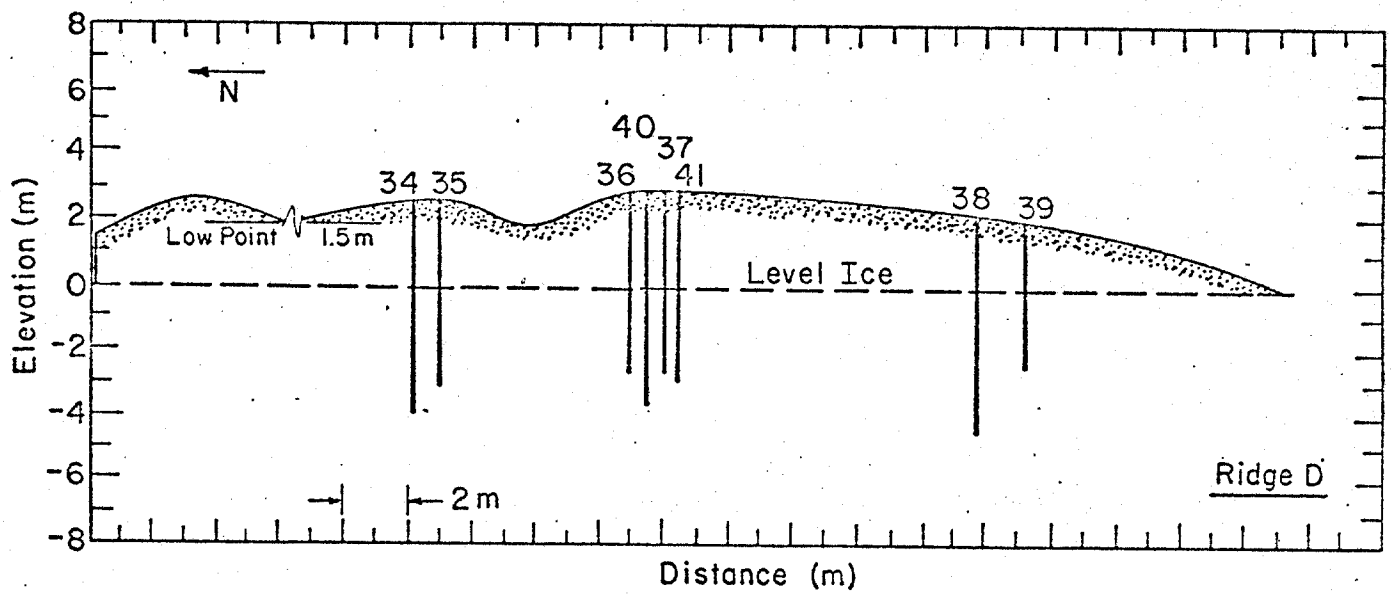

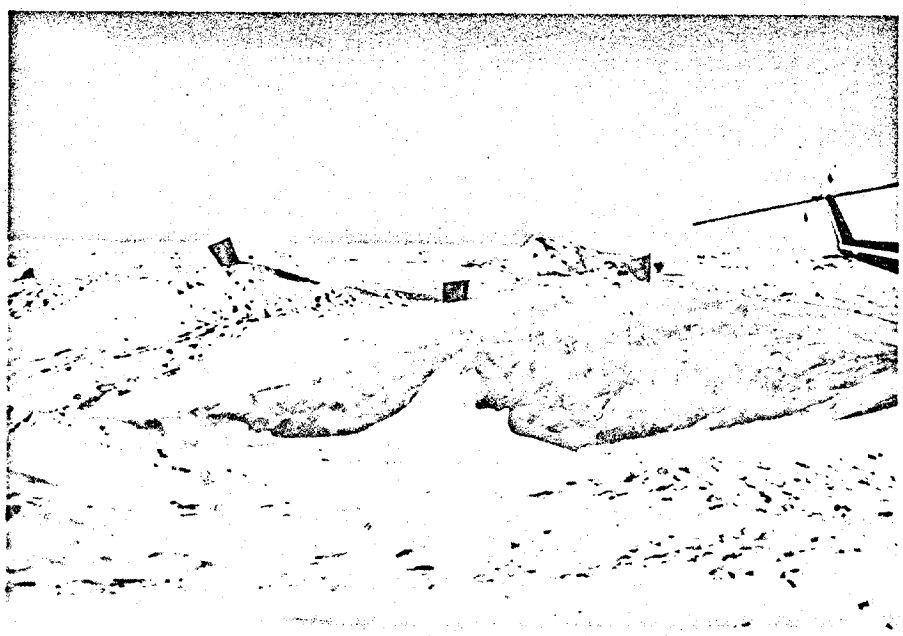

Figure 9: Split end portion of Ridge D.

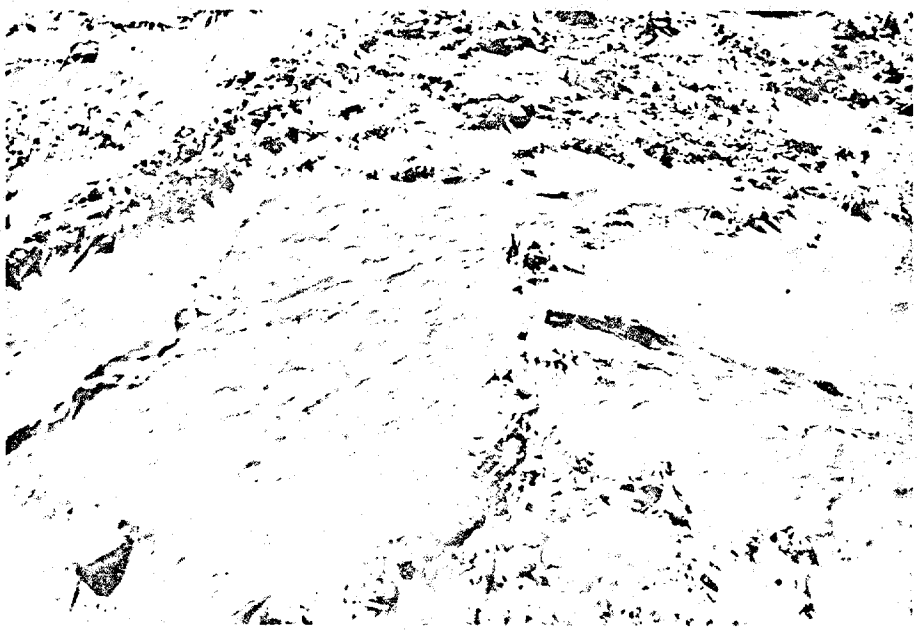

Figure 10: Aerial view of multi-year floe where undeformed samples were obtained.

Table 1 summarizes the estimated height of the top of each core hole above level ice (approximate sea level). Also given is the penetration depth (the total length cored from each hole). Table 2 gives the daily drilling log and Table 3 provides a summary of this data. The primary part of the coring program was carried out with the 4-1/4 in. corer in four days (15-18 April) with a total of 205.6 m of core recovered. The total number of samples (vertical) obtained from this core were 439 or roughly 100 samples per day. The total length of 12 in. diameter core obtained was 12.79 m which resulted in 61 horizontal specimens giving a grand total of 500 specimens for the season. As mentioned we also obtained 8.75 m of core for petrographic studies.

Core Logging Procedures

There were some differences in the core logging procedures between the 1981 and 1982 field seasons. These were the result of two different factors. First, as the result of the Phase I testing program, we had found that some of our field measurements did not prove to be particularly useful. For instance in 1981 we took rather detailed temperature and salinity profiles in the field. As the important temperature is the ice temperature at the time of testing, in 1982 we reduced the temperature measurements in the field to three or four per core, a number sufficient to indicate the general temperature profile in the ice. We also reduced the number of subsidiary salinity measurements as we have not found brine drainage to be an important problem in the low salinity multiyear ice we have been sampling. Also our routine laboratory procedures include a salinity determination on

Table 1. 1982 Ridge Heights and Penetration Depths.

Location	Date		Height	Depth	Height	Depth	Dia.	Remarks
R82A	15 Apr 82	1	230 cm	461 cm	7.7 ft	15.0 ft	4.25 in.	
		2	234 cm	384 cm	7.7 ft	12.6 ft	4.25 in.	
		3	234 cm	473 cm	7.7 ft	14.3 ft	4.25 in.	
		4	300 cm	581 cm	9.8 ft	19.1 ft	4.25 in.	
		5	345 cm	454 cm	11.3 ft	14.9 ft	4.25 in.	
		6	300 cm	502 cm	9.8 ft	16.5 ft	4.25 in.	
		7	234 cm	373 cm	7.7 ft	12.2 ft	4.25 in.	
		8	234 cm	373 cm	7.7 ft	12.2 ft	4.25 in.	
		9	234 cm	377 cm	7.7 ft	12.4 ft	4.25 in.	
		10	503 cm	601 cm	16.5 ft	19.7 ft	4.25 in.	
		11	406 cm	327 cm	13.3 ft	10.7 ft	4.25 in.	
R82B	16 Apr 82	12	203 cm	380 cm	6.7 ft	12.5 ft	4.25 in.	
		13	203 cm	409 cm	6.7 ft	13.4 ft	4.25 in.	
		14	249 cm	472 cm	8.2 ft	15.5 ft	4.25 in.	
		15	218 cm	479 cm	7.2 ft	15.7 ft	4.25 in.	
		16	249 cm	473 cm	8.2 ft	15.5 ft	4.25 in.	
		17	249 cm	482 cm	8.2 ft	15.8 ft	4.25 in.	
		18	234 cm	473 cm	7.7 ft	15.5 ft	4.25 in.	
		19	234 cm	396 cm	7.7 ft	13.0 ft	4.25 in.	
		20	185 cm	361 cm	6.1 ft	11.8 ft	4.25 in.	
		21	185 cm	427 cm	6.1 ft	14.0 ft	4.25 in.	
		22	185 cm	354 cm	6.1 ft	11.6 ft	4.25 in.	
		23	234 cm	326 cm	7.7 ft	10.7 ft	4.25 in.	
R82C	17 Apr 82	24	269 cm	624 cm	8.8 ft	20.5 ft	4.25 in.	
		25	269 cm	639 cm	8.8 ft	21.0 ft	4.25 in.	
		26	234 cm	652 cm	7.7 ft	21.4 ft	4.25 in.	
		27	234 cm	544 cm	7.7 ft	17.8 ft	4.25 in.	
		28	269 cm	565 cm	8.8 ft	18.5 ft	4.25 in.	
		29	269 cm	558 cm	8.8 ft	18.3 ft	4.25 in.	
		30	221 cm	680 cm	7.3 ft	22.3 ft	4.25 in.	
		31	221 cm	576 cm	7.3 ft	18.9 ft	4.25 in.	
		32	173 cm	563 cm	5.7 ft	18.5 ft	4.25 in.	SL163cm/5.3ft
		33	173 cm	470 cm	5.7 ft	15.4 ft	4.25 in.	OD1410cm/46.3ft
R82D	18 Apr 82	34	269 cm	676 cm	8.8 ft	22.2 ft	4.25 in.	
		35	269 cm	564 cm	8.8 ft	18.5 ft	4.25 in.	
		36	300 cm	567 cm	9.8 ft	18.6 ft	4.25 in.	
		37	300 cm	577 cm	9.8 ft	18.9 ft	4.25 in.	
		38	218 cm	682 cm	7.2 ft	22.4 ft	4.25 in.	
		39	218 cm	466 cm	7.2 ft	15.3 ft	4.25 in.	
		40	300 cm	678 cm	9.8 ft	22.2 ft	4.25 in.	
		41	300 cm	583 cm	9.8 ft	19.1 ft	4.25 in.	
R82C	19 Apr 82	42	234 cm	404 cm	7.7 ft	13.3 ft	12 in.	
R82C	20 Apr 82	43	173 cm	389 cm	5.7 ft	12.8 ft	12 in.	SL163cm/5.3ft
		44	173 cm	323 cm	5.7 ft	10.6 ft	12 in.	OD1410cm/46.3ft
		45	173 cm	163 cm	5.7 ft	5.3 ft	12 in.	" "
		46	173 cm	364 cm	5.7 ft	11.9 ft	4.25 in.	" "
		47	173 cm	476 cm	5.7 ft	15.6 ft	4.25 in.	" "
R82C	22 Apr 82	48	173 cm	953 cm	5.7 ft	31.3 ft	4.25 in.	" "
R82E	22 Apr 82	49	30 cm	383 cm	1.0 ft	12.6 ft	4.25 in.	SL53cm/1.7ft OD1920cm/63ft

*SL = Sea level below top of hole
OD = Ocean depth

Table 2. Daily Core Log
1982 Shell Phase Two Field Program

Date	Ridge Location	Hole #	Drill Used	Core Lengths (cm)	Total Depth (m)
4/15/82	R82-A	1	Blue 4-1/4	122, 108, 100, 94, 37	4.62
		2	"	122, 112, 97, 53	3.84
		3	"	119, 115, 98, 66, 39	4.37
		4	"	128, 102, 102, 94, 100, 55	5.81
		5	"	122, 93, 91, 102, 46	4.54
		6	"	126, 104, 100, 96, 76	5.02
		7	"	121, 112, 95, 45	3.73
		8	"	127, 103, 105, 38	3.73
		9	"	125, 106, 99, 47	3.77
		10	"	127, 101, 105, 92, 105, 71	6.01
		11	"	74, 48, 98, 107	3.27
4/16/82	R82-B	12	Blue 4-1/4	127, 105, 56, 32, 40	3.80
		13	"	130, 91, 108, 80	4.09
		14	"	115, 111, 104, 96, 46	4.72
		15	"	118, 107, 106, 98, 50	4.79
		16	"	119, 105, 102, 101, 46	4.73
		17	"	118, 114, 98, 106, 46	4.82
		18	"	121, 105, 110, 92, 45	4.73
		19	"	110, 111, 102, 73	3.96
		20	"	122, 104, 98, 37	3.61
		21	"	121, 116, 103, 87	4.27
		22	"	126, 107, 96, 24	3.54
		23	"	121, 106, 99	3.26
4/17/82	R82-C	24	Orange 4-1/4	105, 113, 100, 106, 102, 98	6.24
		25	"	128, 102, 96, 101, 99, 113	6.39
		26	"	120, 114, 106, 114, 96, 102	6.52
		27	"	120, 126, 120, 80, 98	5.44
		28	"	117, 126, 124, 100, 98	5.65
		29	"	106, 109, 121, 116, 106	5.58
		30	"	114, 123, 100, 123, 110, 110	6.80
		31	"	121, 108, 115, 112, 120	5.76
		32	"	110, 110, 116, 110, 117	5.63
		33	"	126, 107, 121, 116	4.70
4/18/82	R82-D	34	Orange 4-1/4	114, 119, 111, 106, 123, 103	6.76
		35	"	115, 110, 109, 120, 110	5.64
		36	"	110, 117, 122, 113, 105	5.67
		37	"	116, 112, 125, 114, 110	5.77
		38	"	122, 111, 122, 113, 120, 94	6.82
		39	"	121, 112, 112, 121	4.66
		40	"	120, 123, 112, 124, 89, 110	6.78
		41	"	120, 114, 122, 124, 103	5.83
4/19/82	R82-C	42	Blue 12"	96, 82, 100, 60, 66	4.04
4/20/82	R82-C	43	Blue 12"	103, 80, 88, 52, 66	3.89
		44	"	94, 102, 71, 56	3.23
		45	"	101, 62	1.63
		46	Orange 4-1/4	120, 122, 122	3.64
		47	"	121, 117, 124, 114	4.76
4/21/82	No Drilling		High Winds - Blowing Snow		
4/22/82	R82-C	48	Orange 4-1/4	112, 116, 124, 113, 112, 102, 46, 58, 103, 67*	9.53
	R82-E	49	Orange 4-1/4	114, 30, 100, 68, 66*	3.83

*Denotes bottom of pressure ridge.

Table 3. Summary of Daily Drilling.

Date	Drill	# Holes	# Cores	Average Core Length	Total Length of Core Obtained
4/15/82	Blue 4-1/4	11	52	93 cm	48.7 m
4/16/82	Blue 4-1/4	12	53	95 cm	50.32 m
4/17/82	Orange 4-1/4	10	53	110 cm	58.71 m
4/18/82	Orange 4-1/4	8	42	114 cm	47.93 m
4/19/82	Blue 12 in.	1	5	81 cm	4.04 m
4/20/82	Blue 12 in.	3	11	79 cm	8.75 m
	Orange 4-1/4	2	7	120 cm	8.4 m
4/22/82	Orange/Blue 4-1/4	2	13	92 cm	13.36 m

Total Length of 4 in. diameter core obtained - 226.09 m

Total length of 12 in. diameter core obtained - 12.79 m

Longest 4 in. diameter core obtained - 128 cm; hole no. 25

Longest 12 in. diameter core obtained - 103 cm; hole no. 43

each test specimen after testing is complete. It was decided that the number of salinity determinations was more than adequate.

In 1981 we shipped large quantities of extra core back to CRREL for use in petrographic studies. Much of this core had been damaged during extraction when the extended core dogs scored the core sides instead of cleanly breaking the core off at the bottom of the hole. Such core could not be used for test specimens. In 1982 this problem was resolved and very little damaged core was obtained. We also had found that we were able to save sufficient ice from each 33 cm rough test specimen as collected in the field to prepare the necessary subsidiary thin sections. Therefore, it was not necessary to ship extra-long test specimens or to include extra ice from each core. Samples were cut to 33 cm in the field and extra ice was not included. This resulted in a great saving in time and in shipping costs.

Shipping and Storage of Ice Samples

Initially we had planned to use shipping and storage procedures identical with those that were used in 1981. However, because of the delay in going into the field we were not able to arrange for refrigerated storage at Anchorage (the majority of the refrigerated space is owned by fishing companies and the fishing season had started). In retrospect this problem did us a favor as it forced us to change to direct shipping from Deadhorse to Boston, a procedure that was both easier and successful.

Upon bringing the samples in from the field they were stored at ambient temperatures for a maximum period of six days. As the local temperatures were cold, no problems were experienced with brine drainage. The only additional procedure that was necessary was to pack the end of each core tube with paper to prevent damage to the cores while in transit. Six core tubes were sent in each packing box which was charged with 75 lbs of dry ice (the actual weight was somewhat less than this as there was some sublimation of CO_2 during the shipment of dry ice to use from Anchorage). We then shipped the boxes via AIA with consignment to Emery Air Freight in Anchorage. Before the shipment left Deadhorse, Emery was able to reserve space on a Flying Tigers flight to Boston. Emery also handled the transfers between airlines in Anchorage as well as all the additional paper work. It proved to be a very efficient and satisfactory operation. USACRREL personnel finally met the Tigers flight in Boston with a refrigerated truck and transported the ice to Hanover. Spot checks of temperatures within the boxes upon their arrival in Hanover indicated suitably low temperatures (even in one box where the insulation had been pierced by a fork lift). We plan to repeat these procedures during any future sampling operations.

Coring Procedures

Much of the success of the field program should be credited to the efficiency with which our coring equipment obtained the samples. The 4-in. diameter coring augers were, in fact, the same augers that were used in 1981. As mentioned, at that time we experienced difficulty with the core dogs gripping the sample firmly and producing a clean break at the base of

the core. Instead the dogs frequently formed long gouges in the sides of the samples. These gouges were of sufficient depth that such gouged ice could not be used as test specimens. During the 1982 field season this problem was resolved. A newly designed core dog which provided a more aggressive cutting edge replaced last years dogs. Secondly, an inverted impact hammer was designed to give the extension rods a sharp upward impact. This impact both seated the dogs and caused the core to break cleanly. Figure 11 shows the impact hammer in use. A third change was made to the four-inch coring system which included the addition of a short length of helical flighting directly above the augers. This kept the snow from packing into the top of the core and resulted in decreased friction when the core barrel is being removed from the hole. The helical flighting can be seen in Figure 12 and it is believed that this attachment allowed the drillers to obtain longer cores ranging from 100 cm to a maximum 128 cm.

The major new addition to the coring equipment was the development of a 12 in. diameter coring auger system. The auger itself was designed to obtain 12 in. diameter samples up to 1 m in length. The drill, simply stated, is an exploded version of the 4 in. auger. The barrel material is a reinforced fiberglass epoxy pipe. The cutters are attached to an aluminum disc at the bottom of the drill. The auger flights are nylon epoxied webbing. The top drive adapter couples the auger extensions to the auger. Figure 13 shows the auger attached to the winch and drive system. A commercially available gasoline operated post hole digger was modified to provide the rotation and lifting requirements to operate the drill. Figure 14 shows the mobile drill frame winching itself up a pressure ridge. Once the drill

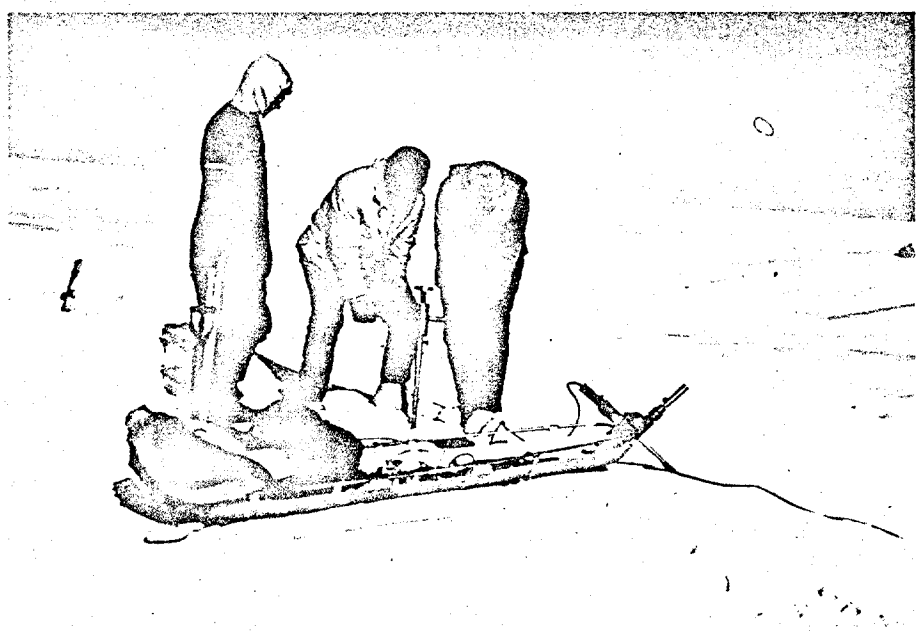

Figure 11: Impact hammer used to engage core dogs and break core.

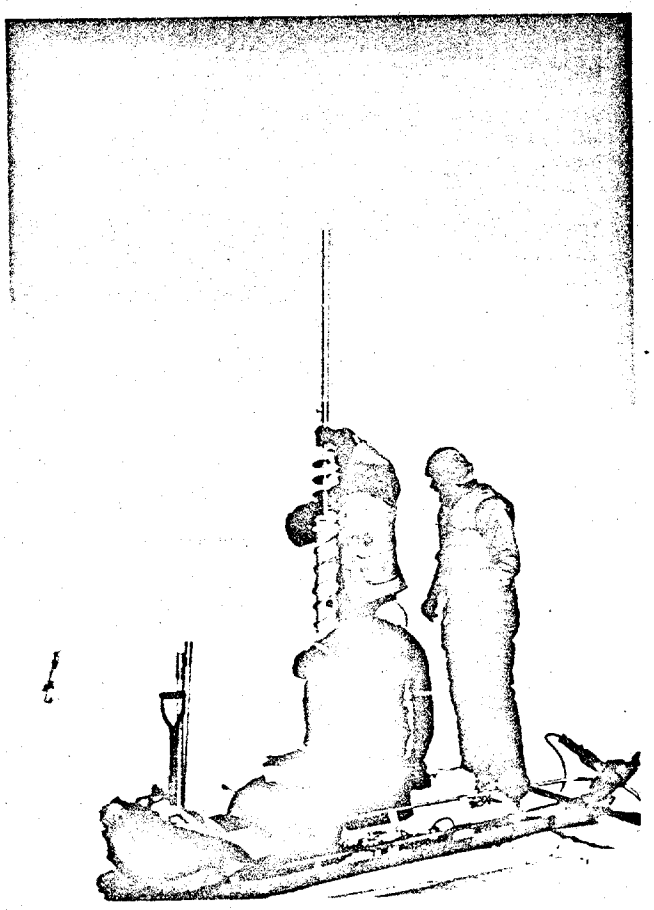

Figure 12: Helical flight on top of core barrel to prevent packing of cuttings above core barrel.

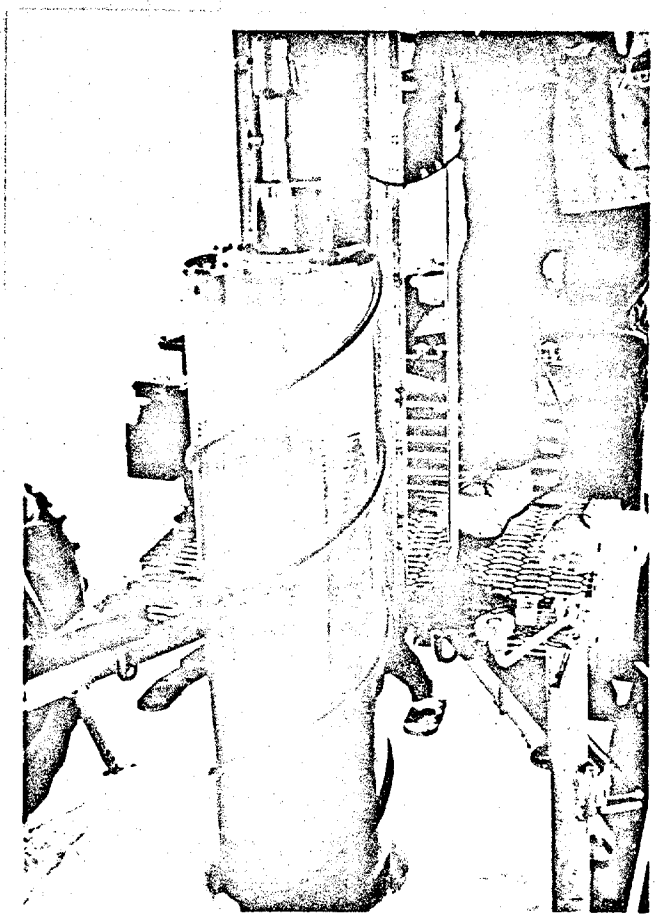

Figure 13: Twelve-inch diameter core barrel.

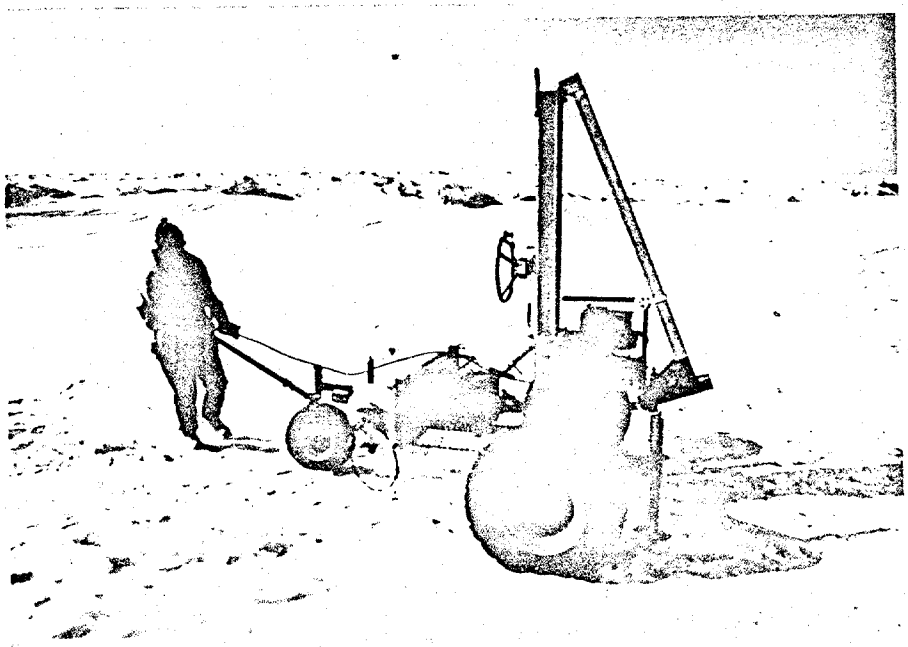

Figure 14: Mobile drilling rig used to support and drive the 12-inch diameter core barrel.

has augered approximately 1 m the drill is removed from the hole. A core retrieval system, Figure 15, is lowered into the hole. A horizontally mounted hydraulic cylinder at the top of this system is activated to shear the core at the bottom. Two core dogs located at the bottom of this device retain the core as it is lifted to the surface. The core is then removed from the retrieval system (Figure 16) and placed in a (log) carrier to move the core to the horizontal sampling drill. To obtain horizontal samples a simple drill press was designed such that 4 in. diameter cores could be obtained from the 12 in. core. Figure 17 shows this system in operation. The only problem encountered with the complete 12 in. system was caused by vibrations when using the horizontal sampling drill. This will be easy to correct in future models by simply adding additional stiffening elements to the drill frame.

The entire 12 in. drilling system was transported to the drilling site by sling loading the mobile frame under the helicopter. Once on the ground a winching system allows the operators to maneuver the system to the exact location desired for drilling. The drilling log is summarized in Table 3.

UNIAXIAL COMPRESSION TESTS

Sampling Scheme and Test Variables

Sixty-two constant strain-rate uniaxial compression tests were performed in Phase II. The tests were conducted at two strain-rates, 10^{-4}/s and 10^{-2}/s, and two temperatures, -20°C and -5°C, to supplement the tests performed in Phase I. In Phase I the compression tests were conducted at strain-rates

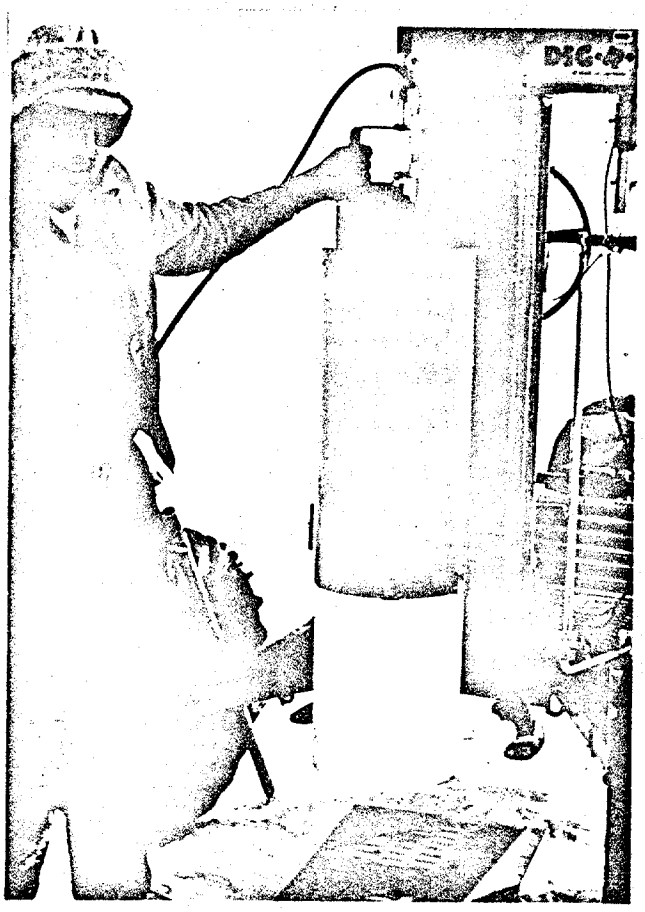

Figure 15: Core catcher used to break and retrieve 12-inch diameter core.

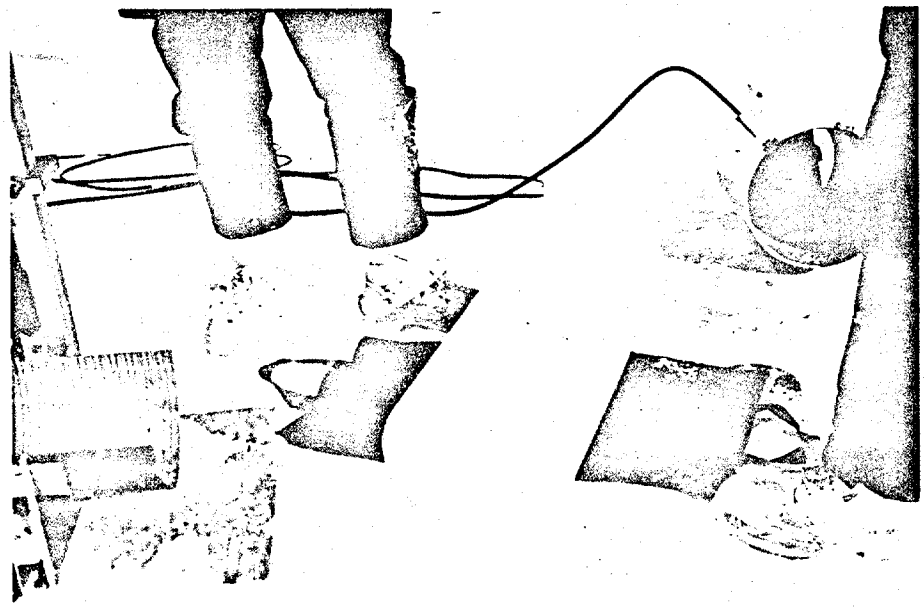

Figure 16: Removing 12-inch diameter core from core catcher.

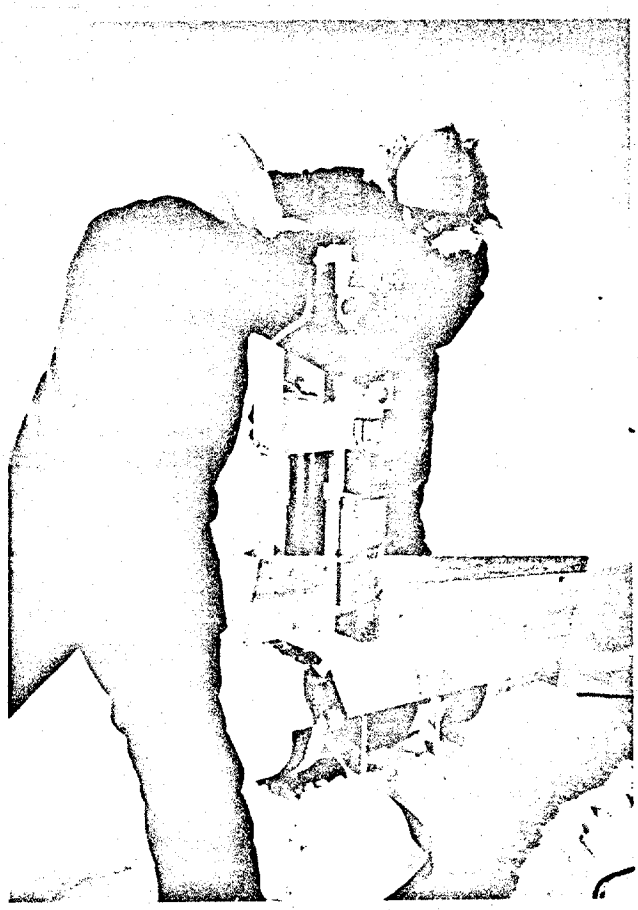

Figure 17: Drill press used to obtain horizontal samples from the 12-inch diameter core.

of 10^{-5}/s and 10^{-3}/s and at temperatures of -20°C and -5°C. Unlike Phase I, tests in Phase II were performed on both horizontal and vertical samples to assess the effect of sample orientation on ice strength. The number of tests at each test condition is summarized in Table 4. Details on the sample preparation and testing techniques are given in Mellor et al. (1983). The procedure used in Phase II were identical to those used in Phase I.

Uniaxial Compressive Strength

A detailed tabulation of the results from the constant strain-rate, uniaxial compression tests is given in Appendix A. The average compressive strength of the ice is plotted against strain-rate in Figure 18 and 19. Figure 18 contains the results from those tests conducted at -5°C (23°F), and Figure 19 presents the results from those tests conducted at -20°C (-4°F). The bars denote one standard deviation from the mean. The test results from Phase I at 10^{-5} and 10^{-3}/s are also included for comparison. Average strength values from Phases I and II are listed in Table 5.

At a given temperature and strain-rate, the Phase II strength data show considerable scatter. Preliminary analyses in Phase I have demonstrated that the large variation in strength can be explained by large variations in the ice structure and porosity.

Based on our understanding of the variation of ice strength with strain-rate we would expect a power law relationship between ice strength and strain-rate in the ductile range (Weeks and Mellor, 1983). On log-log

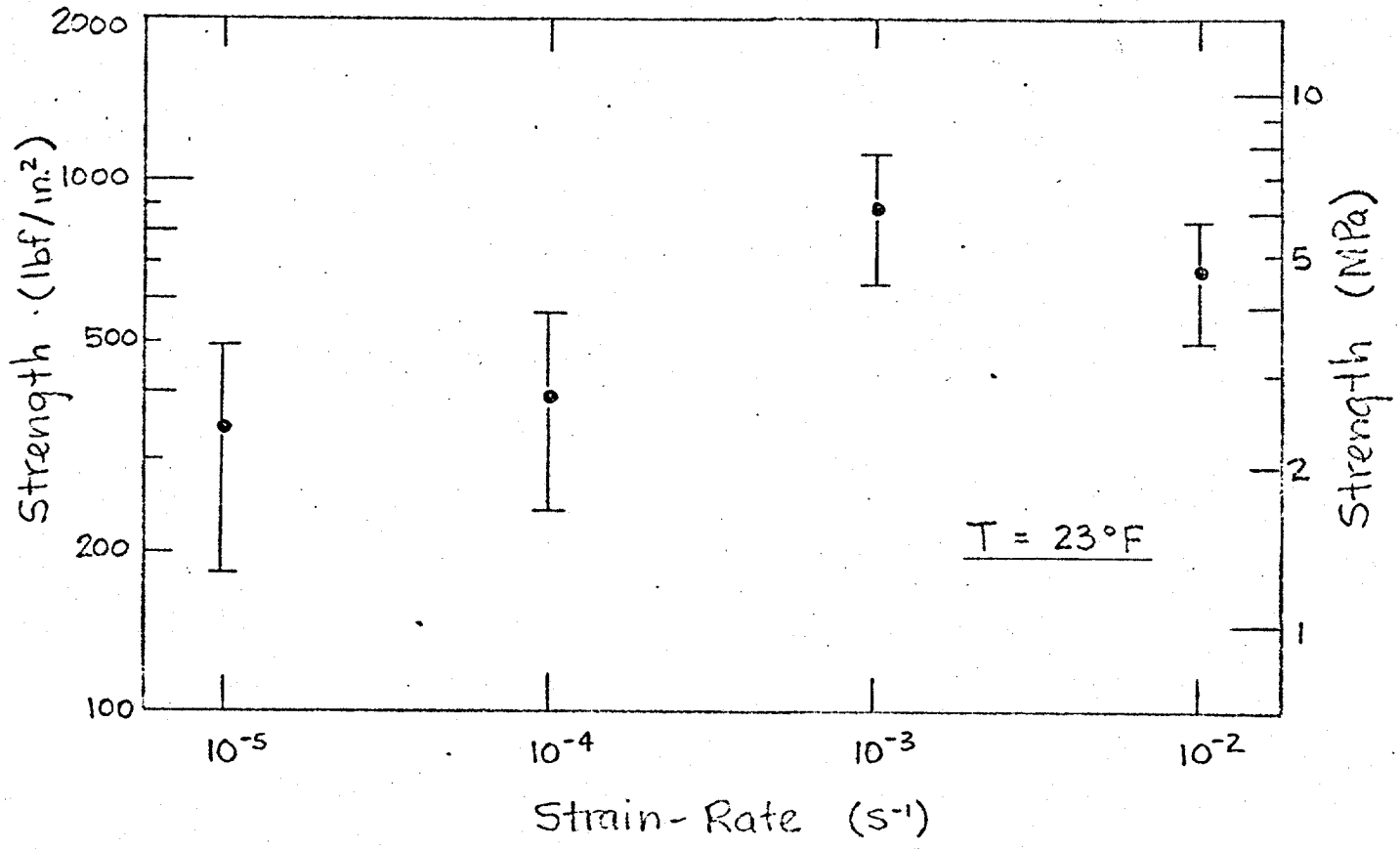

Figure 18: Uniaxial compressive strength versus strain-rate for samples tested at -5°C (23°F). The bars denote one standard deviation.

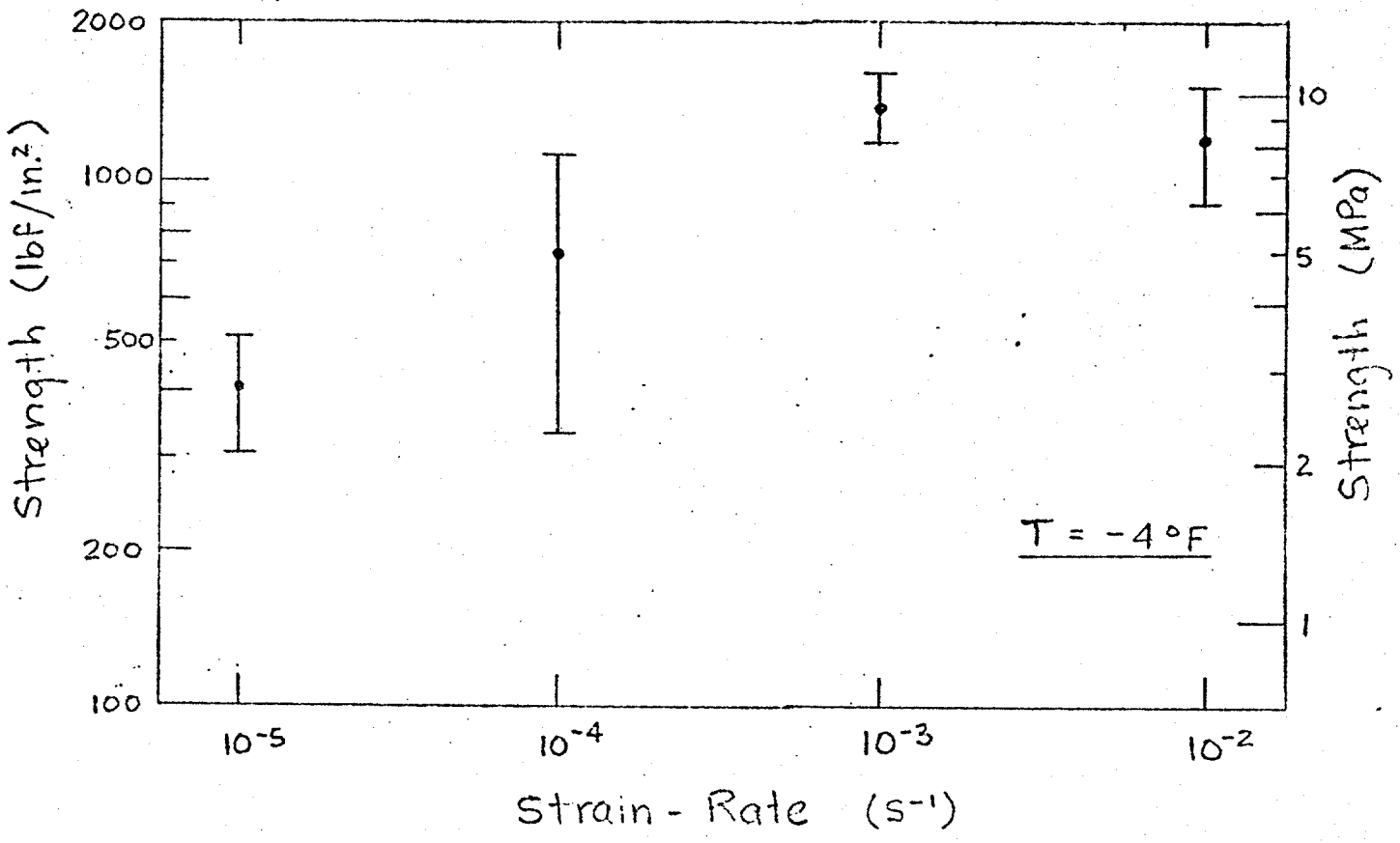

Figure 19: Uniaxial compressive strength versus strain-rate for samples tested at -20°C (-4°F). The bars denote one standard deviation.

Table 4: Number of uniaxial compression tests at different temperatures and strain-rates.

$\dot{\varepsilon}$ / T	10^{-4}/s	10^{-2}/s	
-5°C (23°F)	9V 10H	9V	18V 10H
-20°C (-4°F)	13V 12H	9V	22V 12H
	22V 22H	18V	40V 22H

Table 5: Summary of compressive strength data for Phases I and II.

	Uniaxial Compressive Strength							
	Maximum		Minimum		Mean		Mean Porosity	
	(MPa)	(lbf/in.^{2})	(MPa)	(lbf/in.^{2})	(MPa)	(lbf/in.^{2})	(ppt)	Samples
-5°C (23°F)								
10^{-5}/s V	7.52	1090	0.47	68	2.34±1.08	340±157	44	71
10^{-4}/s V	5.52	800	1.87	271	3.07±1.23	445±179	69	9
10^{-4}/s H	3.87	561	1.21	175	2.35±0.74	341±108	78	10
10^{-4}/s all	5.52	800	1.21	175	2.69±1.04	390±151	73	19
10^{-3}/s V	10.90	1580	2.39	346	6.06±1.63	879±237	46	69
10^{-2}/s V	6.42	931	2.69	390	4.67±1.17	677±169	68	9
-20°C (-4°F)								
10^{-5}/s V	4.26	617	1.17	170	2.79±0.69	404±100	36	41
10^{-4}/s V	12.73	1846	3.34	485	6.17±3.10	894±450	50	13
10^{-4}/s H	7.02	1018	1.68	243	3.74±1.67	543±242	33	12
10^{-4}/s all	12.73	1846	1.68	243	5.00±2.70	725±392	42	25
10^{-3}/s V	12.68	1838	7.03	1020	9.63±1.39	1396±202	39	41
10^{-2}/s V	10.48	1520	4.12	597	8.24±2.05	1195±297	74	9

H - Horizontal V - Vertical

paper, strength versus strain-rate would plot as a straight line. The combined average test results of Phases I and II at -5°C (23°F) do not show this tendency. The average strength of the 10^{-4}/s tests is lower than anticipated. However, at -20°C (-4°F) the 10^{-4}/s Phase II test average is in reasonable agreement with the 10^{-5}/s and 10^{-3}/s averages obtained in Phase I.

Since the strength of sea ice decreases with increasing porosity, it appears that the above observations can be explained in terms of the average ice porosity of the samples tested at each strain-rate and temperature. In Table 5 mean porosities are given for the samples tested at each test condition. It can be seen that at -5°C, the 10^{-4}/s tests have a much higher porosity than the tests conducted at 10^{-5}/s and 10^{-3}/s. At -20°C, the mean porosities of the 10^{-5}/s, 10^{-4}/s, and 10^{-3}/s are similar and the average strength values do show a power law relationship.

In both the -5 and -20°C tests conducted at a strain-rate of 10^{-2}/s, there is an apparent decrease in ice strength relative to the tests conducted at 10^{-3}/s. We attribute this decrease in strength to the much larger porosity of the 10^{-2}/s samples.

Noticeable differences in strength were also found between the horizontal and vertical samples tested at 10^{-4}/s. Generally, the vertical samples had a higher strength. At -5°C (23°F) the average strength of the vertical samples was 30% higher. At -20°C (-4°F) the average strength of the vertical and horizontal samples differred by 65%. While the -5°C (23°F)

vertical samples had a lower porosity, the -20°C (-4°F) vertical samples had a significantly higher porosity. However, the -20°C (-4°F) vertical samples contained two relatively strong specimens (Figure 23) which are believed to be columnar ice samples oriented in the hard fail direction.

The compressive strength of the samples is plotted against the total porosity of the ice in Figures 20 through 23. The air and brine volume equations given in Cox and Weeks (1982) were used to calculate the ice porosity from the ice salinity, temperature, and density. As in Phase I there is a tendency for the ice strength to decrease with increasing porosity. This trend is again most pronounced at high strain-rates, 10^{-2}/s, where flaws and cavities play a more important role in brittle ice behaviour.

Thin sections have been prepared of the horizontal and vertical samples to examine the influence of ice structure on the ice mechanical properties. This analysis should be completed at the end of May and will be included in the draft final report.

Residual Compressive Strength

The uniaxial compression tests on the testing machine were programmed to continue to 5% full sample axial strain to examine the residual strength and post-yield behaviour of the ice. The residual strength is defined as the stress on the sample at 5% strain assuming a constant 10.16 cm (4.000 in.) diameter specimen. Average values of the residual/maximum strength ratio of the ice samples under different loading conditions are given in Table 6. Data from Phase I are included for comparison.

Figure 20: Uniaxial compressive strength versus porosity for tests conducted at -5°C (23°F).

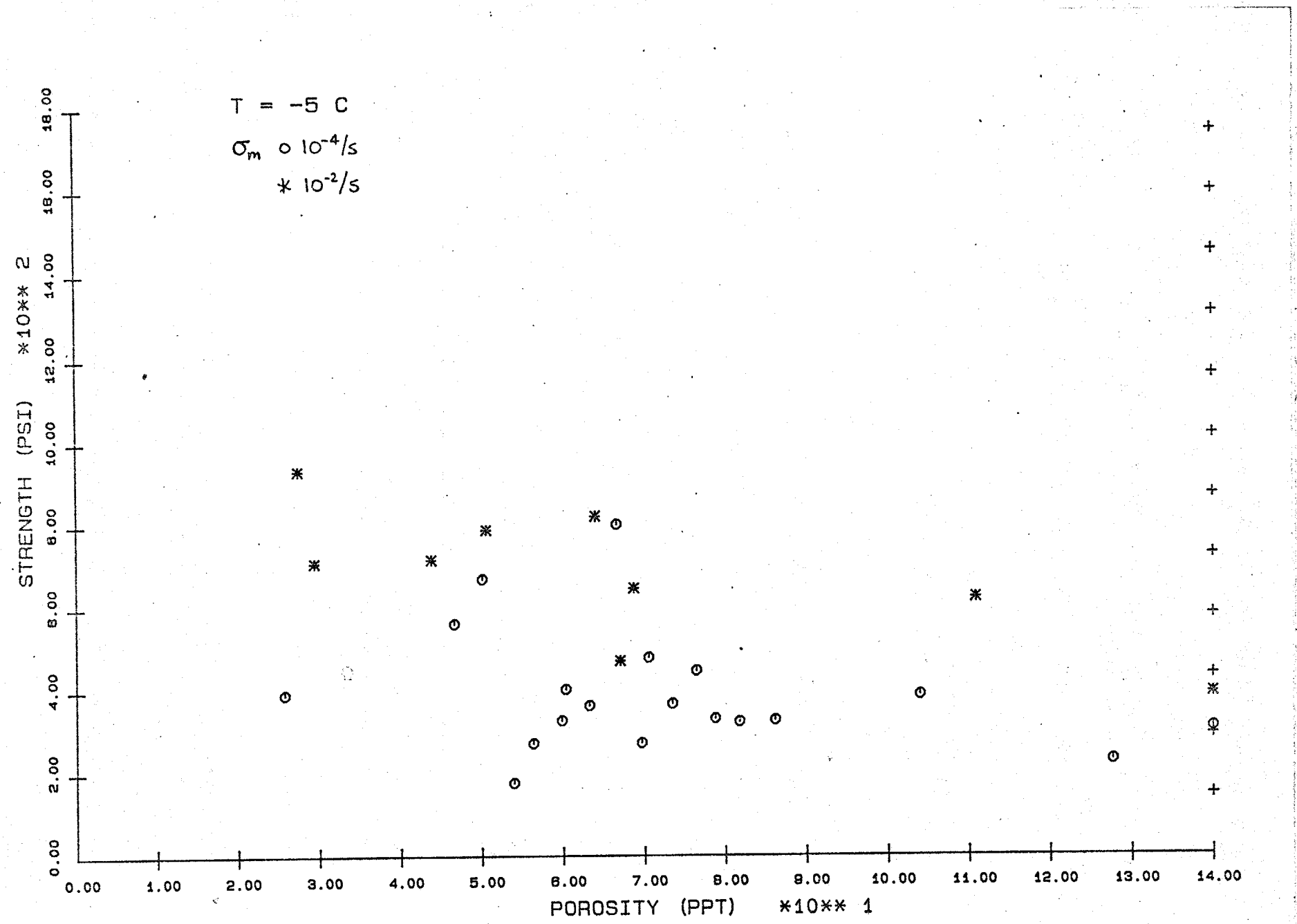
T = -5 C
σ_m o 10^{-4}/s
* 10^{-2}/s
STRENGTH (PSI) *10** 2
0.00
2.00
4.00
6.00
8.00
10.00
12.00
14.00
16.00
18.00
0.00
1.00
2.00
3.00
4.00
5.00
6.00
7.00
8.00
9.00
10.00
11.00
12.00
13.00
14.00
POROSITY (PPT) *10** 1

Figure 21: Uniaxial compressive strength versus porosity for tests conducted at -20°C (-4°F).

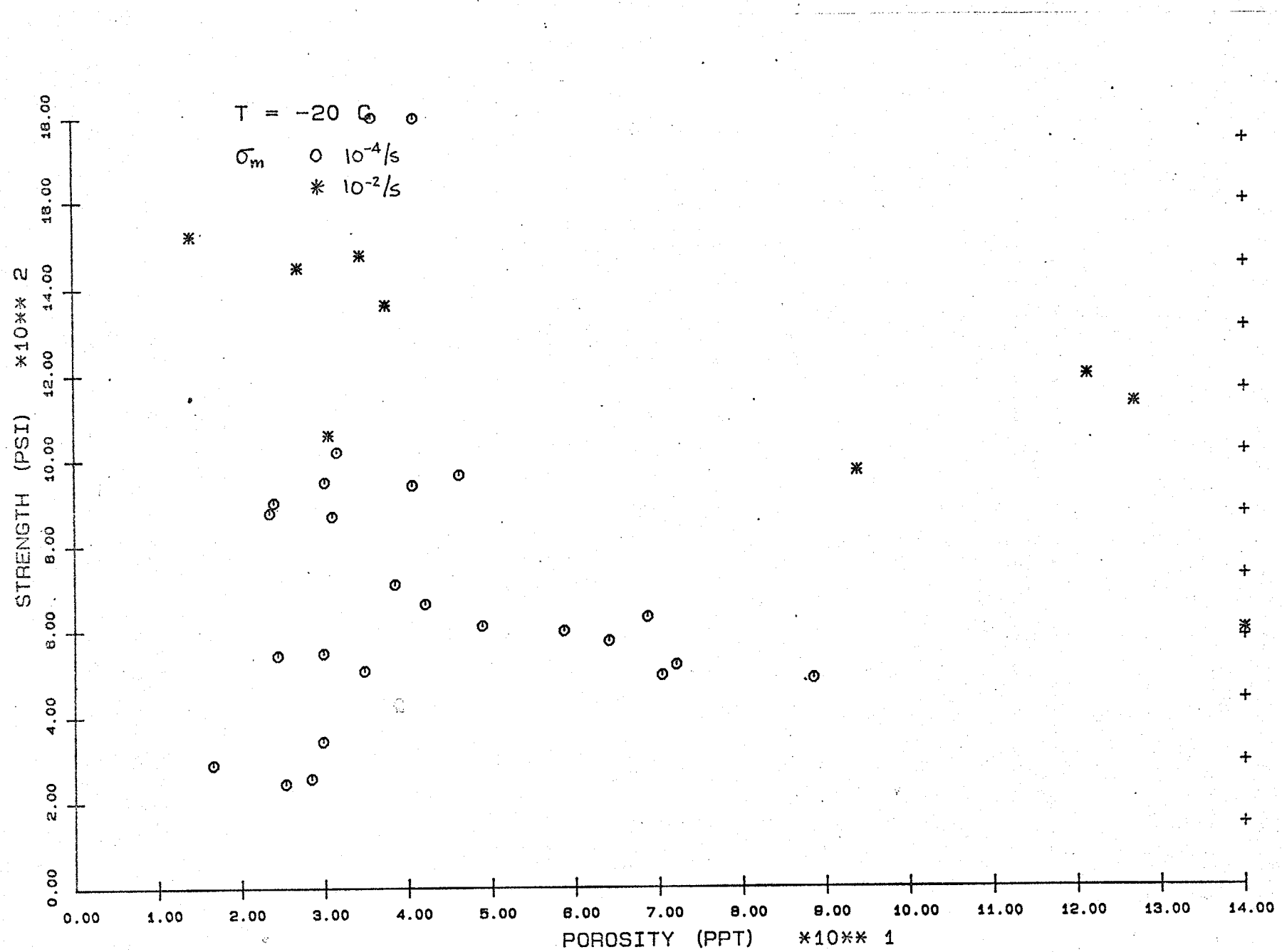
T = −20 C
σm
o 10^-4/s
* 10^-2/s
STRENGTH (PSI) *10** 2
0.00
2.00
4.00
6.00
8.00
10.00
12.00
14.00
16.00
18.00
0.00
1.00
2.00
3.00
4.00
5.00
6.00
7.00
8.00
9.00
10.00
11.00
12.00
13.00
14.00
POROSITY (PPT) *10** 1

Figure 22: Uniaxial compressive strength versus porosity for horizontal and vertical samples tested at -5°C (23°F) and 10^4/s.

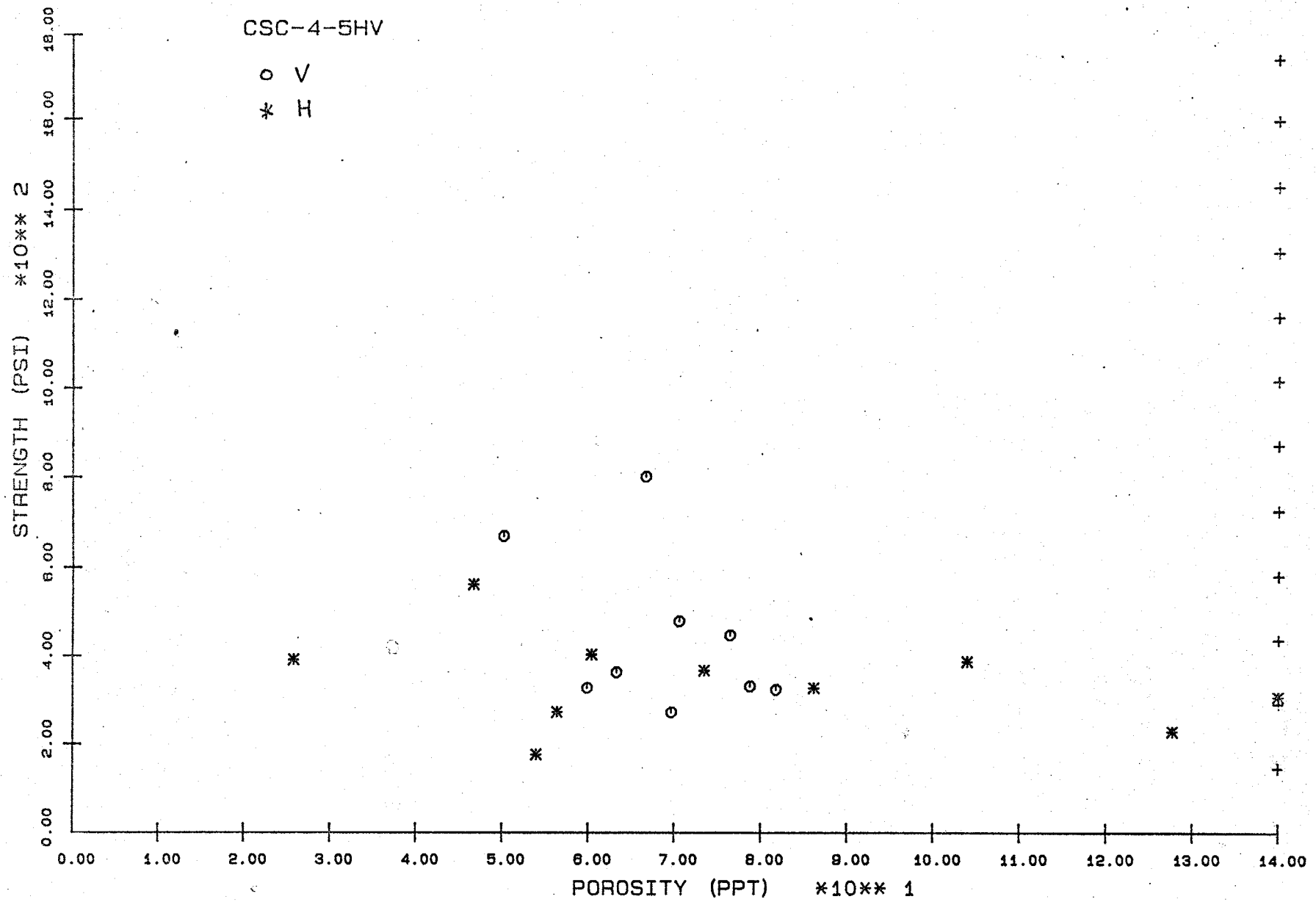
CSC-4-5HV
o V
* H
STRENGTH (PSI) *10** 2
0.00
2.00
4.00
6.00
8.00
10.00
12.00
14.00
16.00
18.00
0.00
1.00
2.00
3.00
4.00
5.00
6.00
7.00
8.00
9.00
10.00
11.00
12.00
13.00
14.00
POROSITY (PPT) *10** 1

Figure 23: Uniaxial compressive strength versus porosity for horizontal and vertical samples tested at -20°C (-4°F) and 10^4/s.

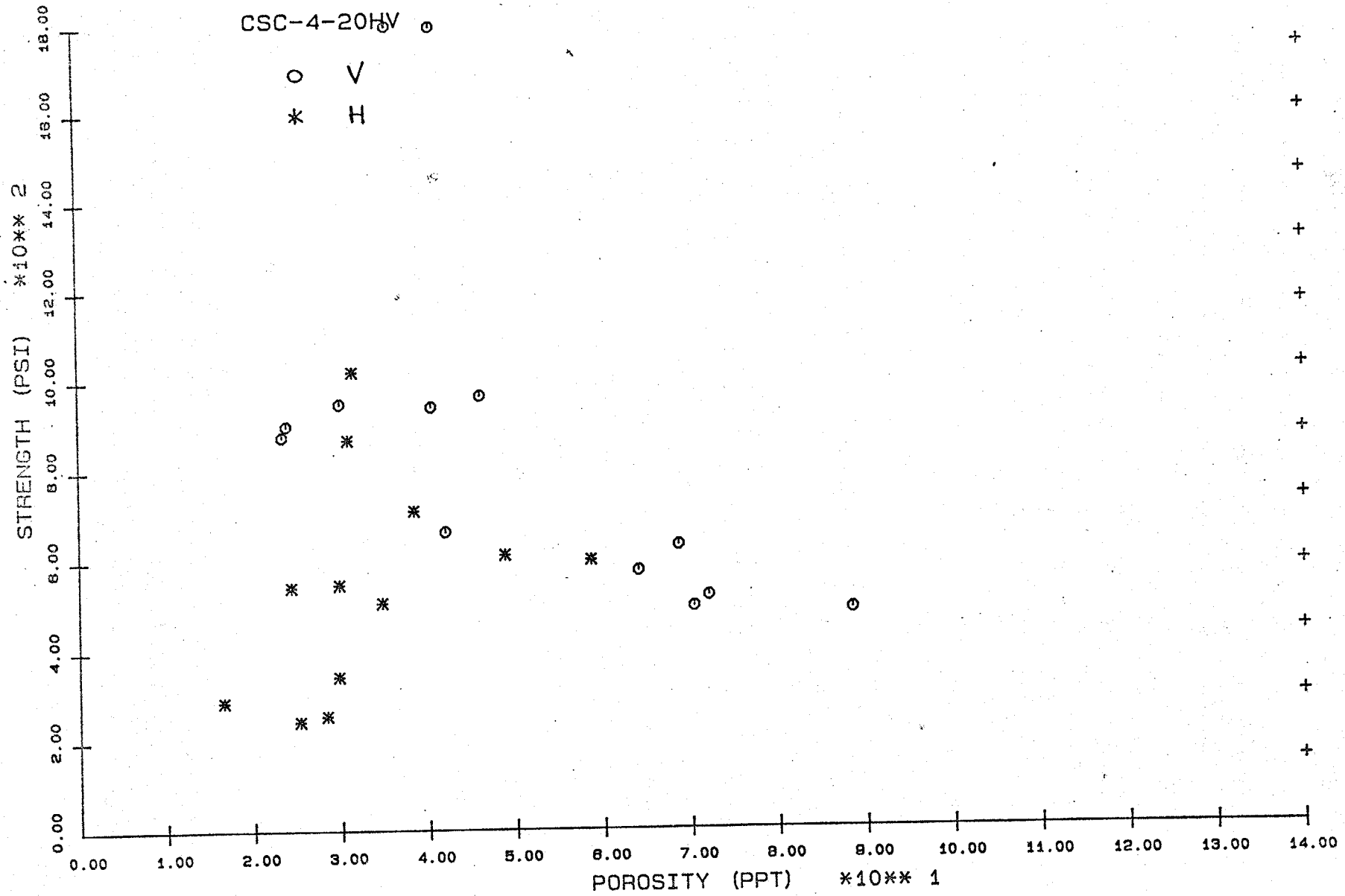
CSC-4-20HV
V
H
STRENGTH (PSI) *10** 2
0.00
2.00
4.00
6.00
8.00
10.00
12.00
14.00
16.00
18.00
0.00
1.00
2.00
3.00
4.00
5.00
6.00
7.00
8.00
9.00
10.00
11.00
12.00
13.00
14.00
POROSITY (PPT) *10** 1

Table 6: Summary of residual/maximum compressive strength ratio data for Phases I and II.

Residual/Maximum Strength Ratios

	Maximum	Minimum	Mean	Samples	Percent to 5% Strain
-5°C(23°F)					
10^{-5}/s V	1.000	0.173	0.688±0.166	68	96
10^{-4}/s V	0.591	0.244	0.396±0.096	9	100
10^{-4}/s H	0.794	0.245	0.439±0.159	10	100
10^{-4}/s all	0.794	0.244	0.418±0.131	19	100
10^{-3}/s V	0.421	0.074	0.198±0.078	43	62
10^{-2}/s V	-	-	-	-	0
-20°C (-4°F)					
10^{-5}/s V	0.970	0.315	0.642±0.162	36	88
10^{-4}/s V	0.504	0.253	0.342±0.077	9	69
10^{-4}/s H	0.675	0.202	0.405±0.137	12	100
10^{-4}/s all	0.675	0.202	0.378±0.114	21	84
10^{-3}/s V	0.746	0.047	0.194±0.148	18	44
10^{-2}/s V	-	-	-	-	0

H - Horizontal V - Vertical

The results show that the residual strength/maximum strength ratio decreases with increasing strain-rate and is relatively insensitive to the ice temperature and porosity. As the strain-rate increases, fewer samples go to 5% strain and at 10^{-2}/s all the tests terminated at the peak or maximum stress.

Failure Strain

Average sample failure strain at the peak or maximum stress for the different test conditions in Phases I and II are given in Table 7. The strains were calculated from the average of the DCDT measurements on the sample. In general, there is a strong tendency for the sample failure strain to decrease with increasing strain-rate. At low strain rates of 10^{-5} and 10^{-4}/s, the failure strain also decreases as the ice gets colder. However, at high strain-rates of 10^{-3} and 10^{-2}/s, the failure strain increases as the ice gets colder. Examination of the standard deviation of the mean strains indicate that the observed temperature trends are not statistically significant.

Strength versus strain to failure plots are given in Figures 24 and 25. At -5°C there is a positive correlation between the strength and failure strain for the 10^{-2}/s tests, whereas at 10^{-4}s, there is no apparent correlation. At -20°C, both the 10^{-4}/s and 10^{-2}/s tests show a positive correlation between the strength and failure strain.

Table 7: Summary of compressive failure strain data for Phases I and II.

	Failure Strain (%)			
	Maximum	Minimum	Mean	Samples
-5°C (23°F)				
10^{-5}/s V	0.83	0.06	0.38±0.17	71
10^{-4}/s V	0.62	0.09	0.18±0.17	9
10^{-4}/s H	0.26	0.06	0.12±0.07	10
10^{-4}/s all	0.62	0.06	0.14±0.12	19
10^{-3}/s V	0.20	0.05	0.13±0.03	69
10^{-2}/s V	0.10	0.02	0.07±0.02	9
-20°C (-4°F)				
10^{-5}/s V	0.73	0.10	0.31±0.14	41
10^{-4}/s V	0.21	0.10	0.15±0.04	13
10^{-4}/s H	0.14	0.07	0.10±0.03	12
10^{-4}/s all	0.21	0.07	0.13±0.04	25
10^{-3}/s V	0.25	0.05	0.19±0.04	41
10^{-2}/s V	0.16	0.08	0.12±0.03	9

H - Horizontal V - Vertical

Figure 24: Uniaxial compressive strength versus failure strain for those tests conducted at -5°C (23°F).

T = -5 C
O 10**-4/s
* 10**-2/s
STRENGTH (PSI) *10**-2
GAUGE LENGTH STRAIN (%) *10**-1
0.00
0.25
0.50
0.75
1.00
1.25
1.50
1.75
2.00
2.25
2.50
2.75
3.00
3.25
3.50

Figure 25: Uniaxial compressive strength versus failure strain for those tests conducted at -20°C (-4°F).

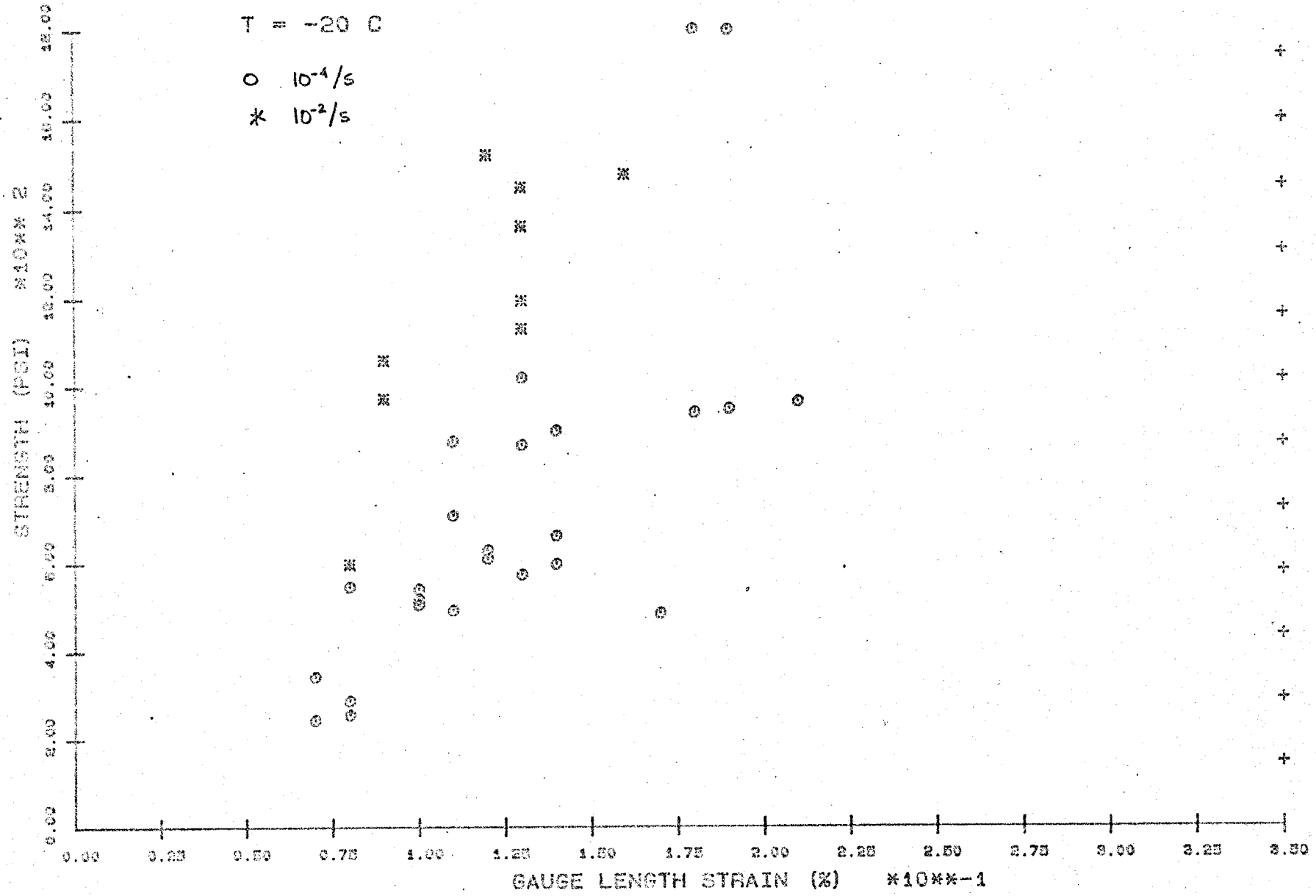
T = -20 C
o 10^{-4}/s
* 10^{-2}/s
STRENGTH (PSI) *10**2
0.00
2.00
4.00
6.00
8.00
10.00
12.00
14.00
16.00
0.00
0.25
0.50
0.75
1.00
1.25
1.50
1.75
2.00
2.25
2.50
2.75
3.00
3.25
3.50
GAUGE LENGTH STRAIN (%) *10**-1

Initial Tangent Modulus

Estimates of the initial tangent modulus were obtain from the initial slope of the force-displacement curves using the same procedures as in Phase I. The results are plotted against strain-rate in Figures 26 and 27 and listed in Table 8. Modulus values from Phase I are included in both the figures and table for comparison. The initial tangent modulus is plotted against the ice porosity for ice temperatures of -5°C and -20°C in Figures 28 and 29, respectively.

It is interesting to note that the initial tangent modulus approaches the "dynamic" Young's modulus of the ice at a lower strain-rate in the colder -20°C tests. Furthermore, at a given strain-rate and temperature there is a tendency for the modulus to decrease with increasing porosity.

Poisson's Ratio

As in Phase I a MTS circumferential strain measurement kit was used to provide estimates of Poisson's ratio. At the conclusion of the compression tests the data were reduced and it was found that the Poisson's ratios from Phase II were much lower than those obtained in Phase I. For example, at -5°C and 10^{-4}/s the average Poisson's ratio at the start of the test was 0.08 ± 0.05. At -5°C and 10^{-3}/s in Phase I we obtained 0.21 ± 0.14. It was initially assumed that the Phase II values were lower because the samples were more porous and compressible. However, we were suspicious in that the Phase I samples having a high porosity did not generally have a low Poisson's ratio. Data reduction, calibration, and recording procedures for the circumferential strain measurements were first reviewed. As no

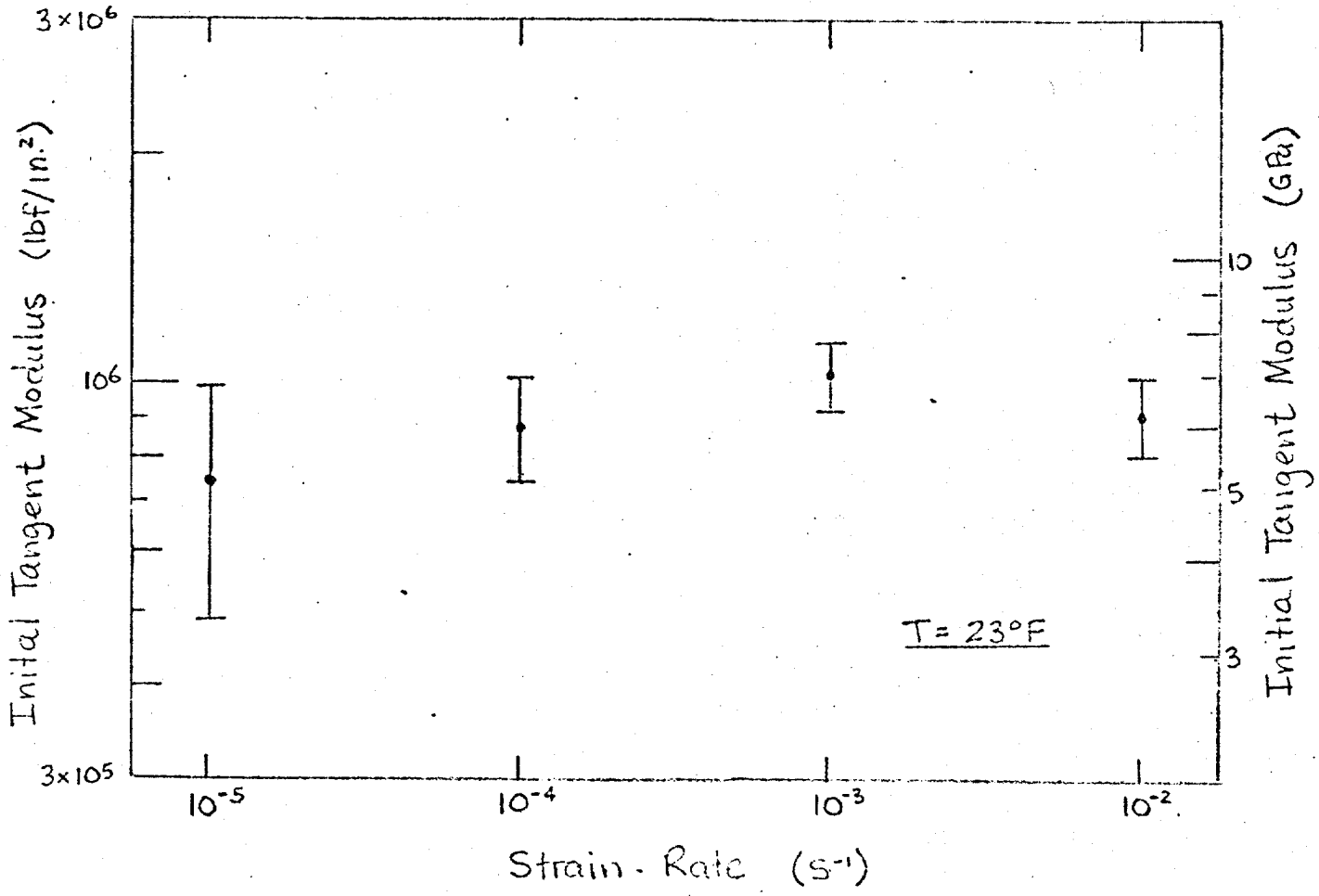

Figure 26: Initial tangent modulus in compression versus strain rate for those tests conducted at -5°C (23°F). The bars denote one standard deviation.

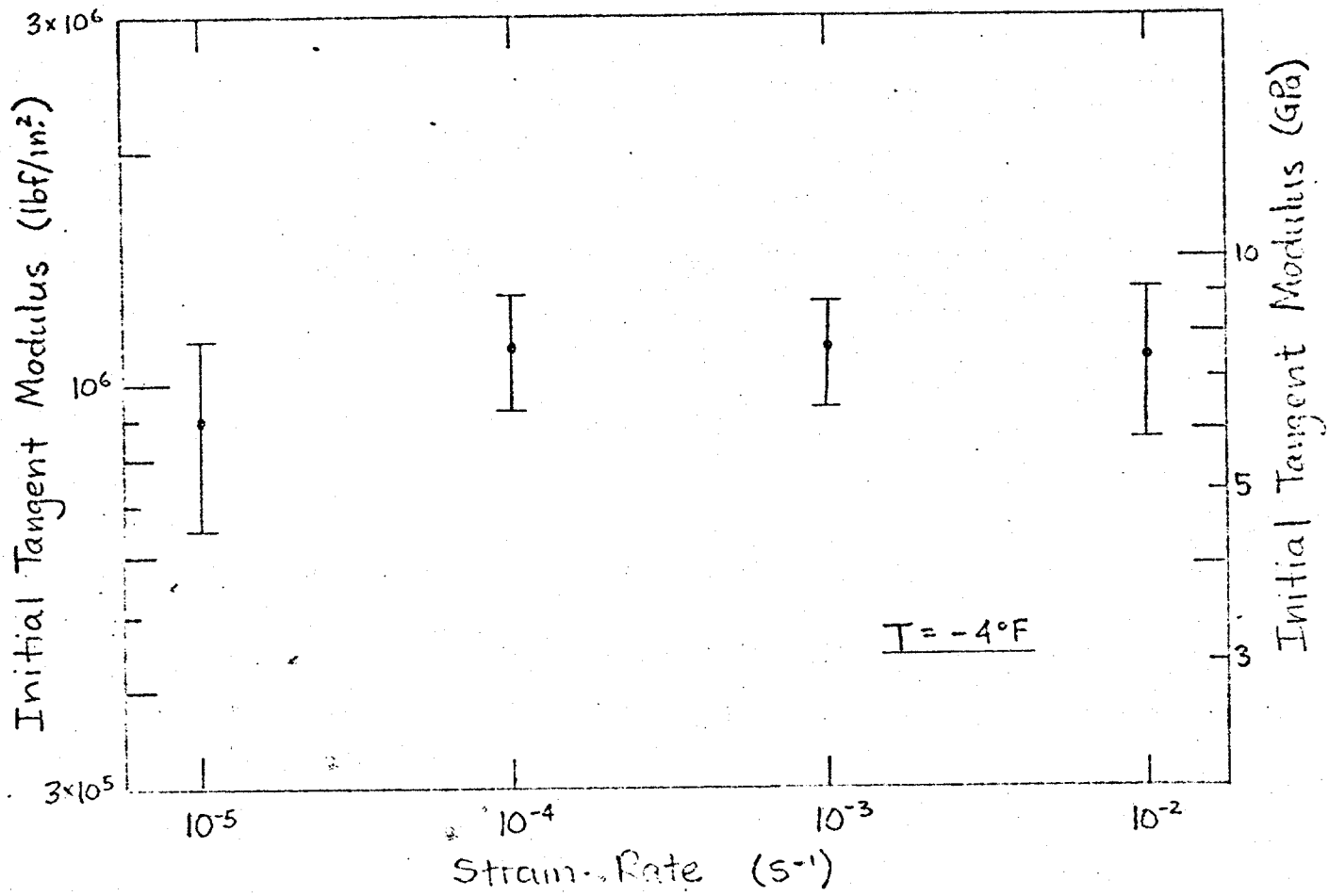

Figure 27: Initial tangent modulus in compression versus strain-rate for those tests conducted at -20°C (-4°F). The bars denote one standard deviation.

Table 8: Summary of compressive initial tangent modulus for Phases I and II.

	Initial Tangent Modulus							
	Maximum		Minimum		Mean		Mean Porosity	
	(GPa)	(lbf/in.^{2}x10^6)	(GPa)	(lbf/in.^{2}x10^6)	(GPa)	(lbf/in.^{2}x10^6)	(ppt)	Sampl
-5°C (23°F)								
10^{-5}/s V	11.45	1.660	2.41	0.350	5.11±1.74	0.741±0.252	44	71
10^{-4}/s V	7.89	1.144	5.32	0.771	6.30±0.96	0.914±0.139	69	9
10^{-4}/s H	7.41	1.074	4.41	0.639	5.81±0.94	0.842±0.136	78	10
10^{-4}/s all	7.89	1.144	4.41	0.639	6.04±0.95	0.876±0.138	73	19
10^{-3}/s V	14.00	2.030	4.95	0.718	7.07±1.38	1.025±0.200	46	71
10^{-2}/s V	6.90	1.000	4.89	0.709	6.21±0.73	0.901±0.106	68	9
-20°C (-4°F)								
10^{-5}/s V	13.79	2.000	3.45	0.500	6.14±1.68	0.890±0.244	36	41
10^{-4}/s V	9.70	1.406	5.35	0.776	7.74±1.42	1.122±0.206	50	13
10^{-4}/s H	10.28	1.490	6.18	0.896	7.58±1.26	1.099±0.182	33	12
10^{-4}/s all	10.28	1.490	5.35	0.776	7.66±1.29	1.111±0.187	42	25
10^{-3}/s V	10.38	1.570	4.89	0.709	7.62±1.19	1.105±0.173	39	40
10^{-2}/s V	10.50	1.522	5.28	0.765	7.50±1.61	1.088±0.233	74	9

H - Horizontal V - Vertical

Figure 28: Initial tangent modulus in compression versus porosity for those tests conducted at -5°C (23°F).

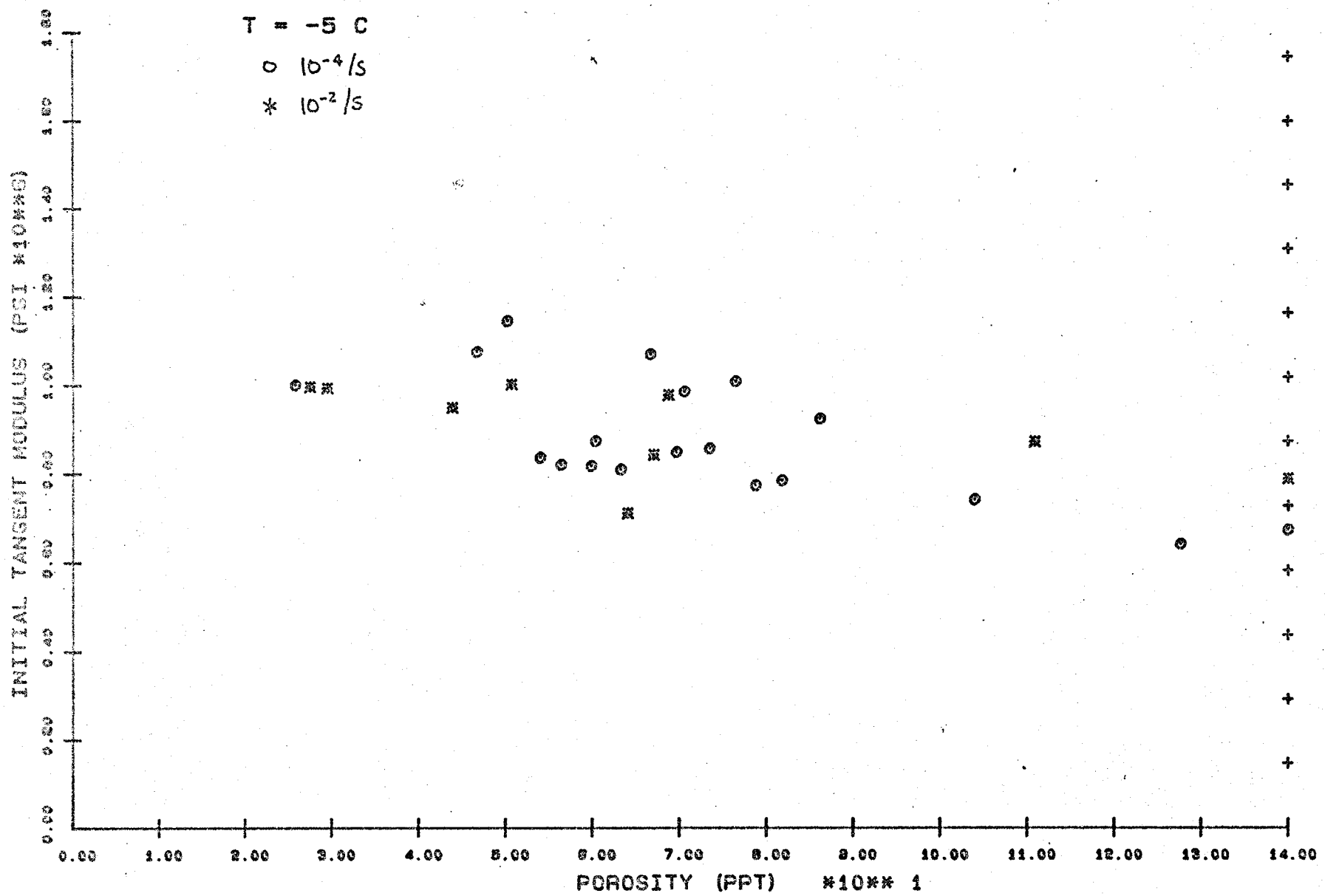
T = -5 C
o 10^{-4}/s
* 10^{-2}/s
INITIAL TANGENT MODULUS (PSI *10**6)
0.00
0.20
0.40
0.60
0.80
1.00
1.20
1.40
1.60
1.80
0.00
1.00
2.00
3.00
4.00
5.00
6.00
7.00
8.00
9.00
10.00
11.00
12.00
13.00
14.00
POROSITY (PPT) *10** 1

Figure 29: Initial tangent modulus in compression versus porosity for those tests conducted at -20°C (-4°F).

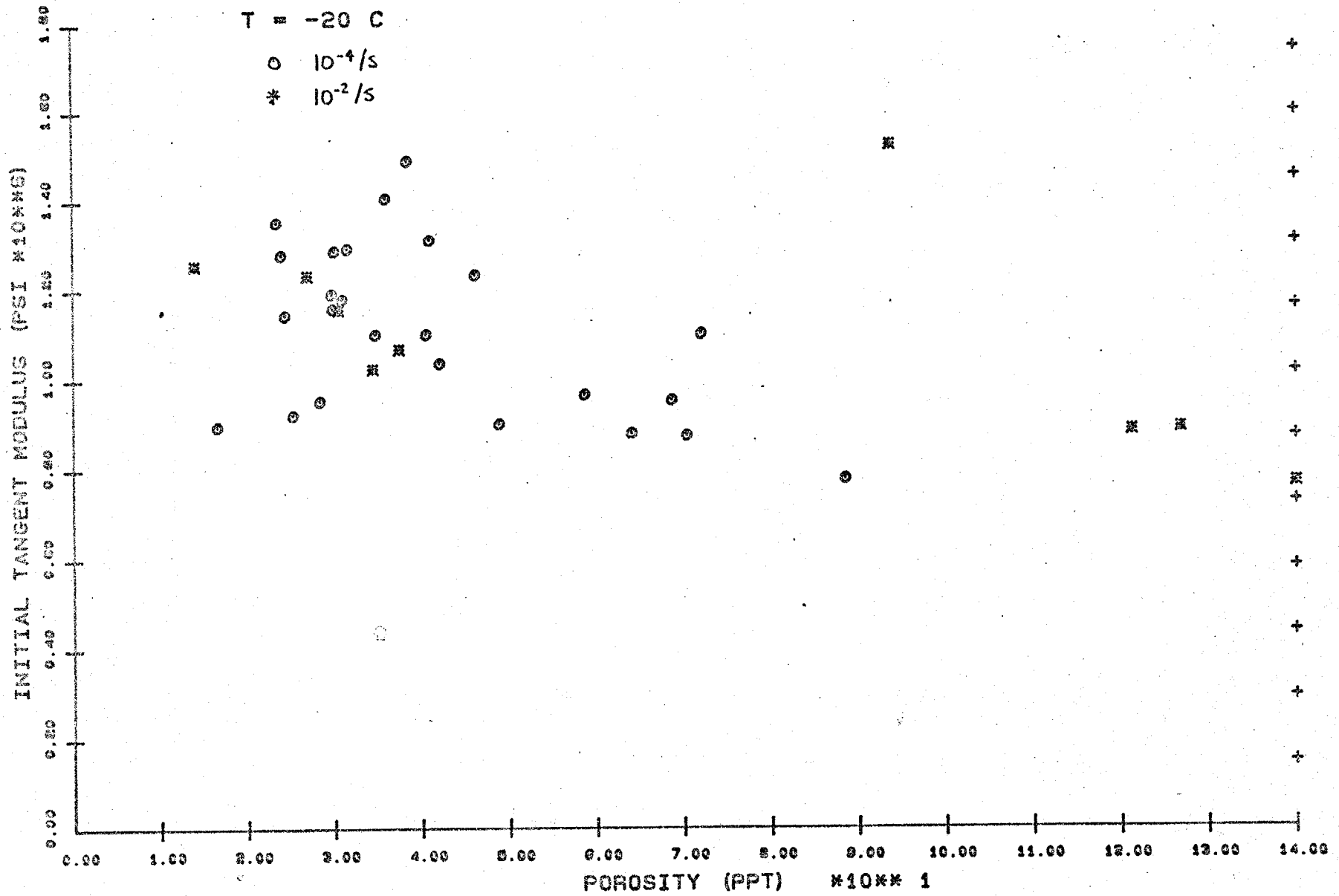
T = -20 C
o 10⁻⁴/s
* 10⁻²/s
INITIAL TANGENT MODULUS (PSI *10**6)
0.00
0.20
0.40
0.60
0.80
1.00
1.20
1.40
1.60
1.80
0.00
1.00
2.00
3.00
4.00
5.00
6.00
7.00
8.00
9.00
10.00
11.00
12.00
13.00
14.00
POROSITY (PPT) *10** 1

irregularities were found, eight Phase I specimens were tested. To our disappointment we again obtained low Poisson's ratio values. It appeared that we had a mechanical problem with the circumferential strain kit. An aluminum cylinder was then fabricated, instrumented with axial DCDTs and the circumferential strain kit, and tested on the MTS machine. While the measured Young's modulus was correct, Poisson's ratio was low and non-linear. We found that to properly use the circumferential strain kit, it is necessary to support the circumferential strain extensometer. This did not prove to be an easy task and after numerous attempts with elastic bands, we stopped trying. Slight movements of the extensometer during loading resulted in erroneous measurements.

As a result of the above findings, no Poisson's ratio data will be provided in Phase II. Poisson's ratio data will also be removed from the Phase I report. In subsequent tests, it will be necessary to properly support the circumferential strain extensometer, or devise an alternate method to measure lateral deformation of the sample.

UNIAXIAL TENSION TESTS

Sampling Scheme and Test Variables

Thirty-six constant strain-rate uniaxial tension tests were performed on vertically oriented multi-year pressure ridge samples in Phase II. The tests were conducted at two strain-rates, 10^{-5}/s and 10^{-3}/s, and at two temperatures, -20°C and -5°C. The number of tests at each test condition is summarized in Table 9. Details on the sample preparation and testing

Table 9: Number of uniaxial tension tests at different temperatures and strain-rates.

$\dot{\varepsilon}$ / T	10^{-5}/s	10^{-3}/s	
-5°C (23°F)	9V	9V	18V
-20°C (-4°F)	9V	9V	18V
	18V	18V	36V

techniques are given in Mellor et al. (1983). The procedures used in Phase II were identical to those in Phase I with the exception that, for on the ice axial strains, the DCDT gauge length was increased from 4.0 in. (10.2 cm) to 4.5 in. (1.4 cm). In Phase I tension tests were performed on samples from a multi-year floe and this data cannot be grouped with the Phase II ridge data.

Uniaxial Tensile Strength

A detailed tabulation of the results from the constant strain-rate uniaxial tension tests is given in Appendix B. The average tensile strength of the ice is plotted against strain-rate in Figures 30 and 31. Figure 30 contains the results from those tests conducted at -5°C (23°F), and Figure 31 presents the results from those tests conducted at -20°C (-4°F). The bars denote one standard deviation from the mean. Average tensile strength values are also listed in Table 10.

In general, the tensile strength shows very little variation with strain-rate or temperature. The lower mean strength obtained at 10^{-3}/s and -5°C (23°F) is probably due to the higher porosity of the samples.

The tensile strength is plotted against the ice porosity in Figures 32 and 33. Disregarding variations in the ice structure there is a tendency for the ice strength to decrease with increasing porosity.

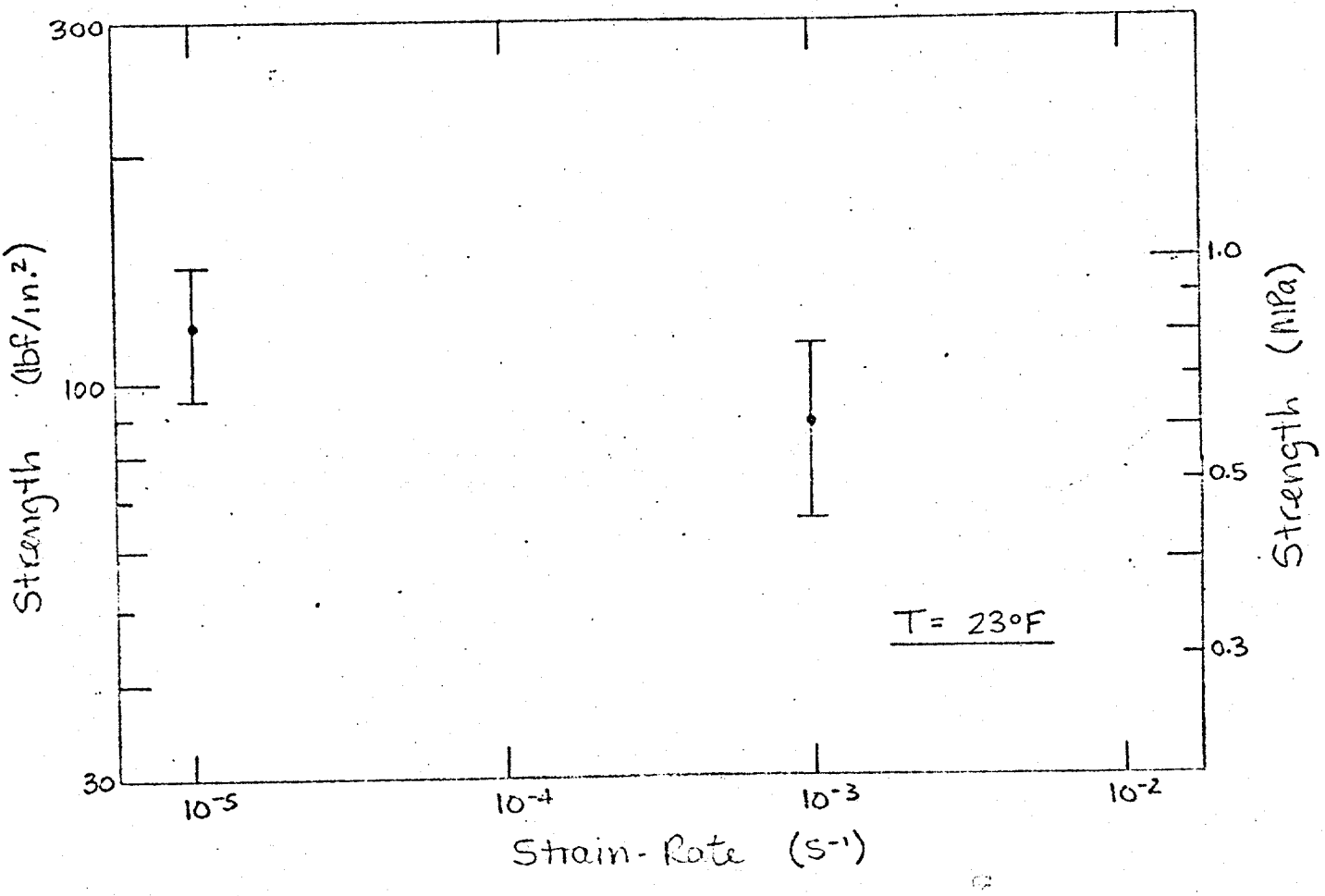

Figure 30: Uniaxial tensile strength versus strain-rate for those tests conducted at -5°C (23°F). The bars denote one standard deviation.

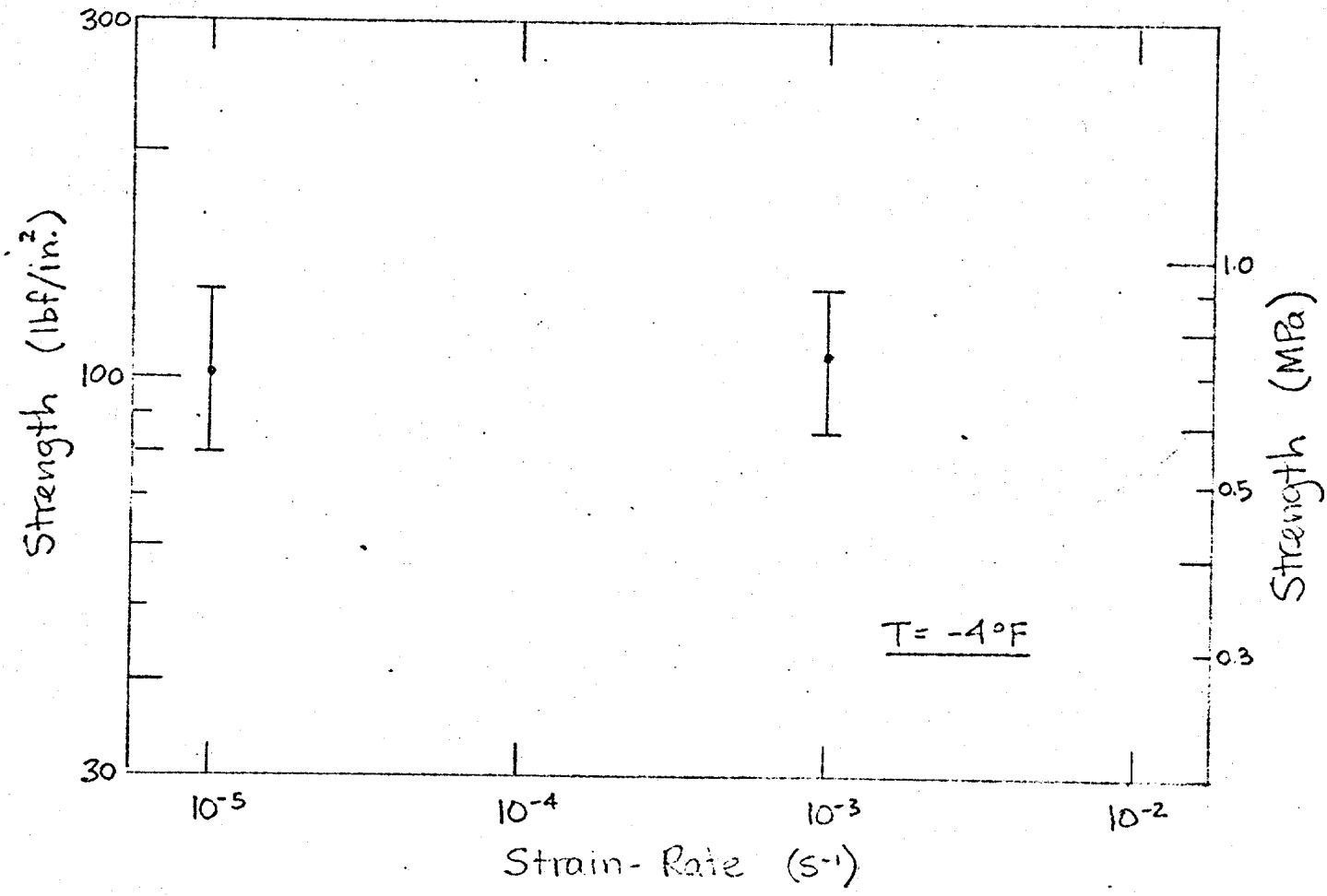

Figure 31: Uniaxial tensile strength versus strain-rate for those tests conducted at -20°C (-4°F). The bars denote one standard deviation.

Table 10: Summary of tensile strength data for Phases II.

Uniaxial Tensile Strength

	Maximum (MPa)	Maximum (lbf/in.^{2})	Minimum (MPa)	Minimum (lbf/in.^{2})	Mean (MPa)	Mean (lbf/in.^{2})	Mean Porosity (ppt)	Samples
-5°C (23°F)								
10^{-5}/s V	1.03	149	0.57	82	0.82±0.17	119±24	78	9
10^{-3}/s V	0.83	120	0.41	60	0.61±0.16	89±23	108	9
-20°C (-4°F)								
10^{-5}/s V	0.92	134	0.49	71	0.71±0.16	103±23	82	9
10^{-3}/s V	0.92	134	0.48	69	0.75±0.16	109±23	77	9

V - Vertical

Figure 32: Uniaxial tensile strength versus ice porosity for those tests conducted at -5°C (23°F).

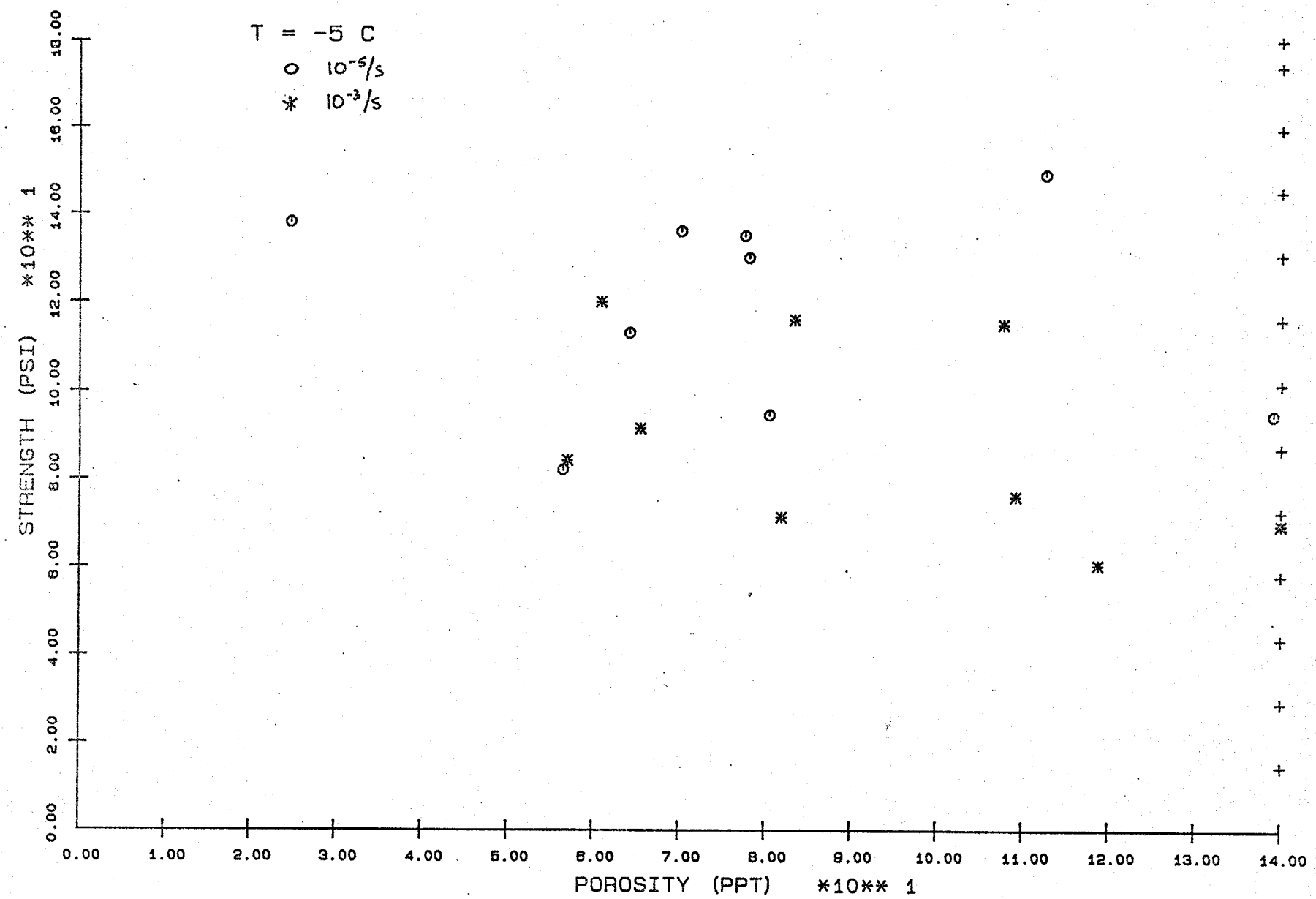
T = -5 C
o 10^-5/s
* 10^-3/s
STRENGTH (PSI) *10** 1
0.00
2.00
4.00
6.00
8.00
10.00
12.00
14.00
16.00
18.00
0.00
1.00
2.00
3.00
4.00
5.00
6.00
7.00
8.00
9.00
10.00
11.00
12.00
13.00
14.00
POROSITY (PPT) *10** 1

Figure 33: Uniaxial tensile strength versus ice porosity for those tests conducted at -20°C (-4°F).

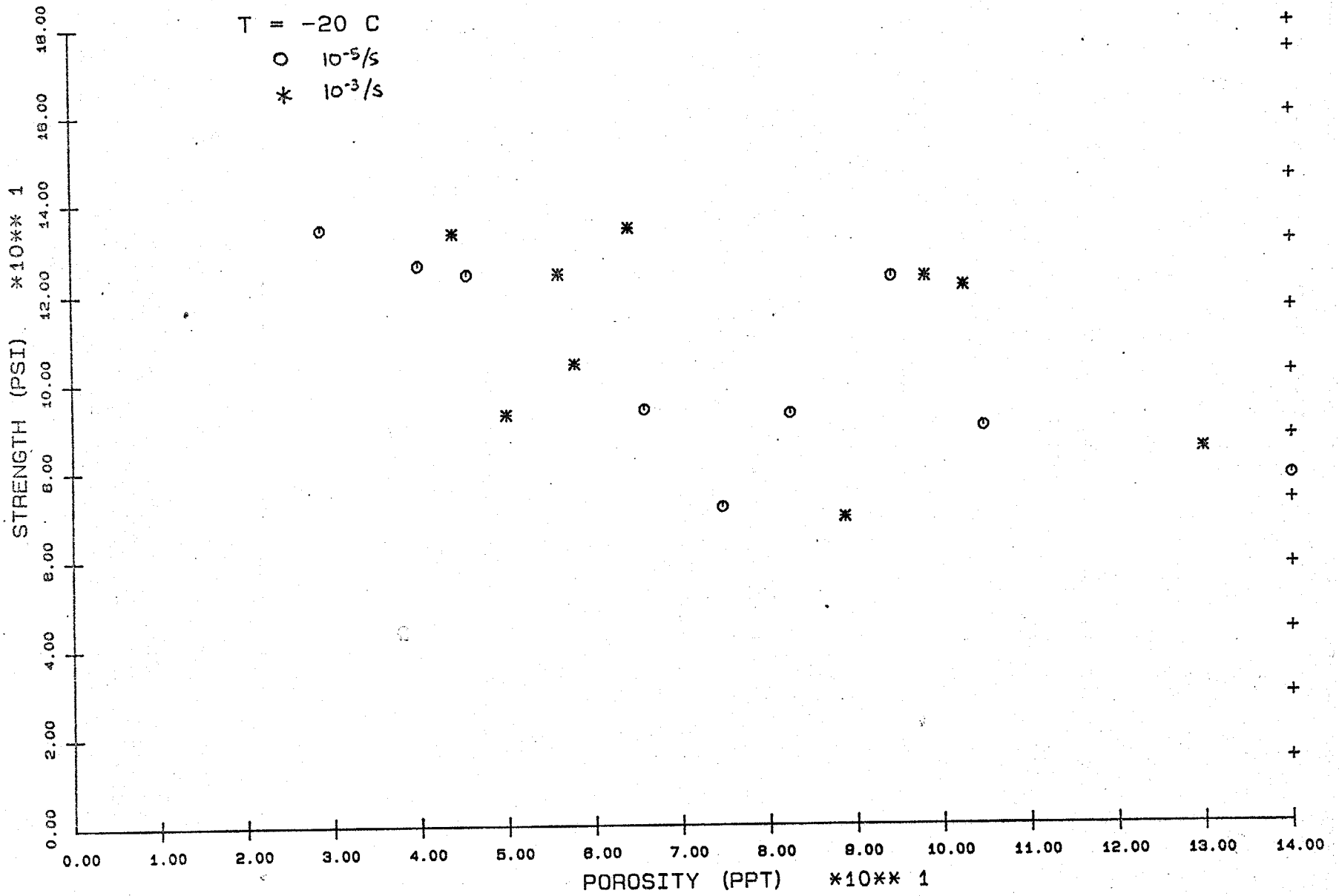
T = -20 C
O 10^-5/s
* 10^-3/s
STRENGTH (PSI) *10** 1
0.00
2.00
4.00
6.00
8.00
10.00
12.00
14.00
16.00
18.00
0.00
1.00
2.00
3.00
4.00
5.00
6.00
7.00
8.00
9.00
10.00
11.00
12.00
13.00
14.00
POROSITY (PPT) *10** 1

Failure Strains

Average tensile failure strains at the peak or maximum stress for each test condition are given in Table 11. In general, the samples failed at 0.01 to 0.02% strain.

Initial Tangent Modulus

Estimates of the initial tangent modulus were obtained from the initial slope of the force-displacement curves. The results are plotted against strain-rate in Figures 34 and 35 and listed in Table 12. The modulus is also plotted against the ice porosity in Figures 36 and 37.

The initial tangent modulus shows a slight increse with increasing strain-rate, and a slight decrease with increasing temperature and porosity. Relative to the compressive initial tangent modulus variations are small.

Table 11: Summary of tensile failure strain data for Phase II.

	Failure Strain (%)			
	Maximum	Minimum	Mean	Samples
-5°C (23°F)				
10^{-5}/s V	0.022	0.014	0.019±0.002	9
10^{-3}/s V	0.013	0.007	0.010±0.002	9
-20°C (-4°F)				
10^{-5}/s V	0.022	0.009	0.013±0.004	9
10^{-3}/s V	0.012	0.009	0.011±0.001	9

V - Vertical

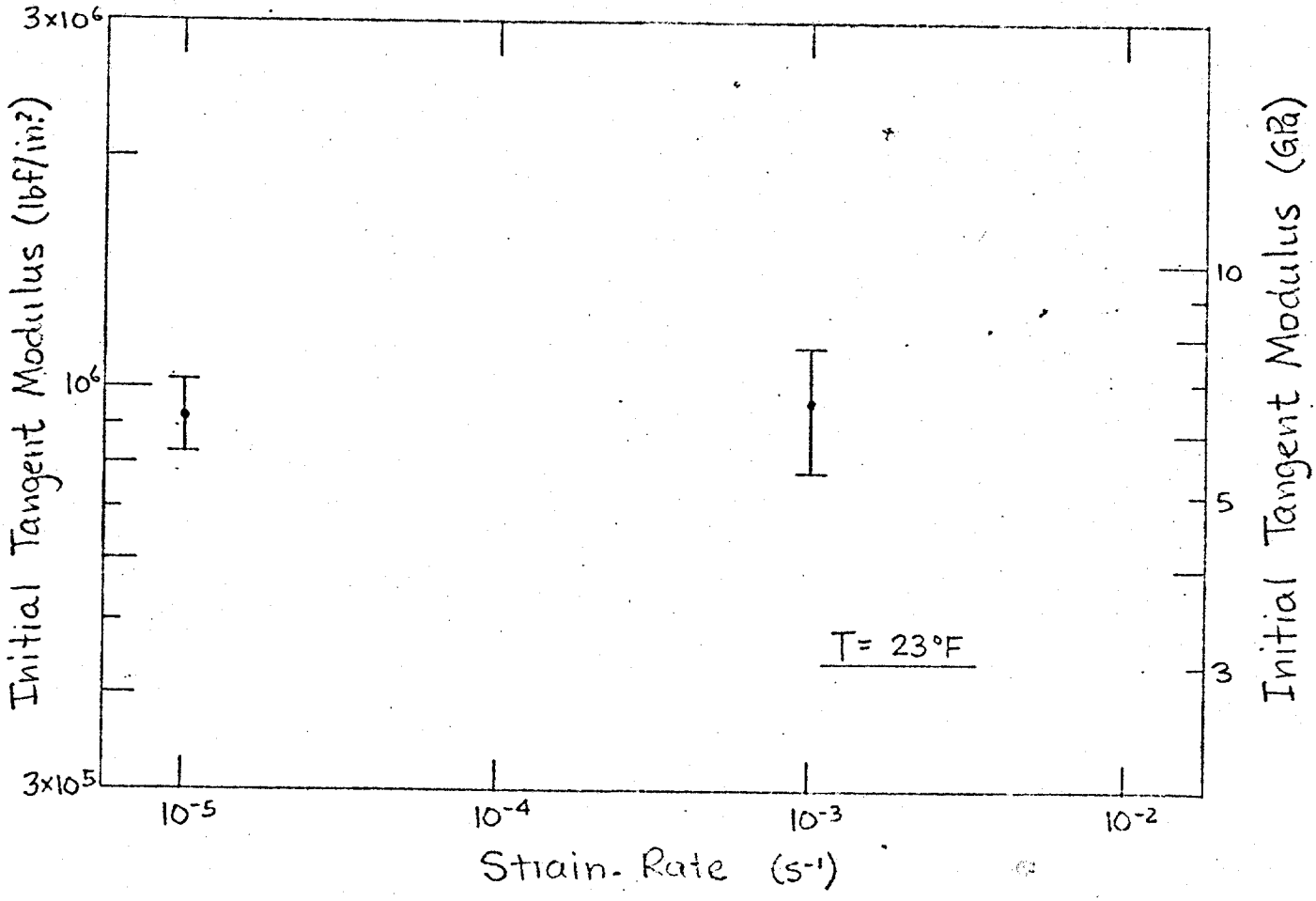

Figure 34: Initial tangent modulus in tension versus strain rate for those tests conducted at -5°C (23°F).

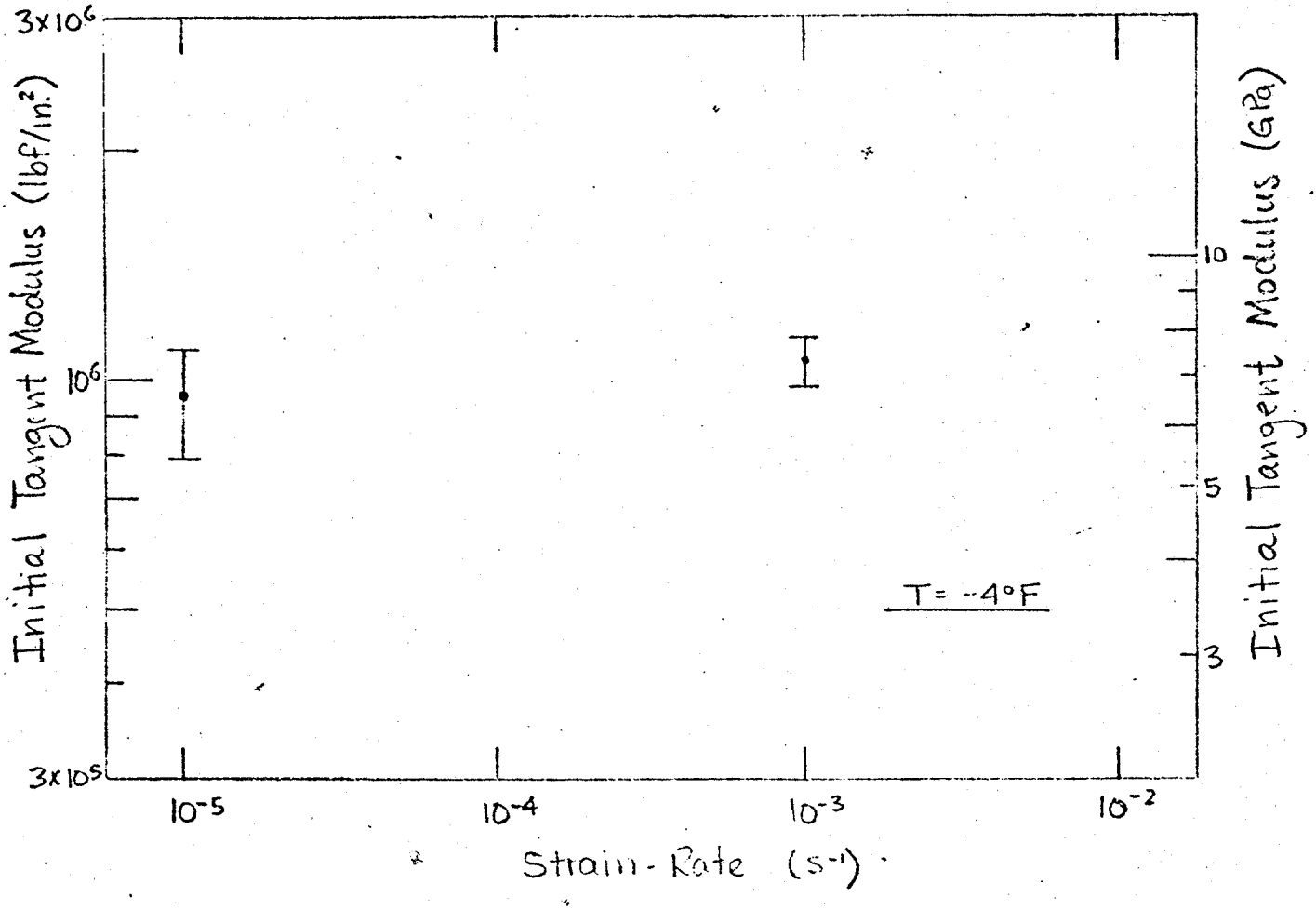

Figure 35: Initial tangent modulus in tension versus strain-rate for those tests conducted at -20°C (-4°F).

Table 12: Summary of tensile initial tangent modulus data for Phase II.

	Initial Tangent Modulus							
	Maximum		Minimum		Mean		Mean Porosity	
	(GPa)	(lbf/ in.^{2}x10^6)	(GPa)	(lbf/ in.^{2}x10^6)	(GPa)	(lbf/ in.^{2}x10^6)	(ppt)	Samples
-5°C (23°F)								
10^{-5}/s V	7.59	1.100	5.42	0.786	6.39±0.68	0.927±0.099	78	9
10^{-3}/s V	8.32	1.207	4.25	0.616	6.60±1.19	0.957±0.173	108	9
-20°C (-4°F)								
10^{-5}/s V	7.82	1.134	4.17	0.604	6.54±1.12	0.949±0.162	82	9
10^{-3}/s V	8.12	1.177	6.59	0.955	7.31±0.54	1.060±0.079	77	9

V - Vertical

Figure 36: Initial tangent modulus in tension versus porosity for those tests conducted at -5°C (23°F).

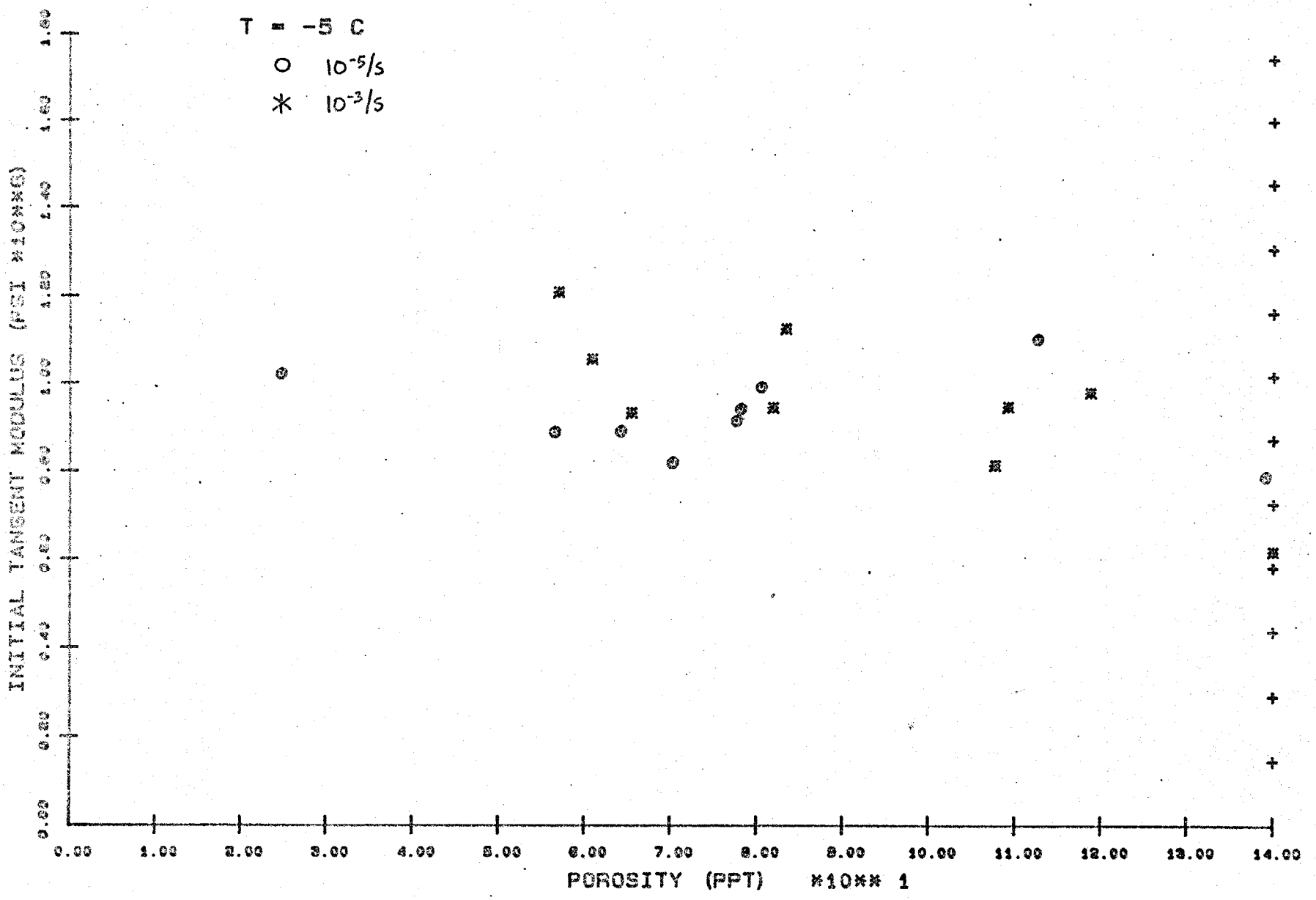
T = -5 C
O 10⁻⁵/s
* 10⁻³/s
INITIAL TANGENT MODULUS (PSI *10**6)
0.00
0.20
0.40
0.60
0.80
1.00
1.20
1.40
1.60
1.80
0.00
1.00
2.00
3.00
4.00
5.00
6.00
7.00
8.00
9.00
10.00
11.00
12.00
13.00
14.00
POROSITY (PPT) *10** 1

Figure 37: Initial tangent modulus in tension versus porosity for those tests conducted at -20°C (-4°F).

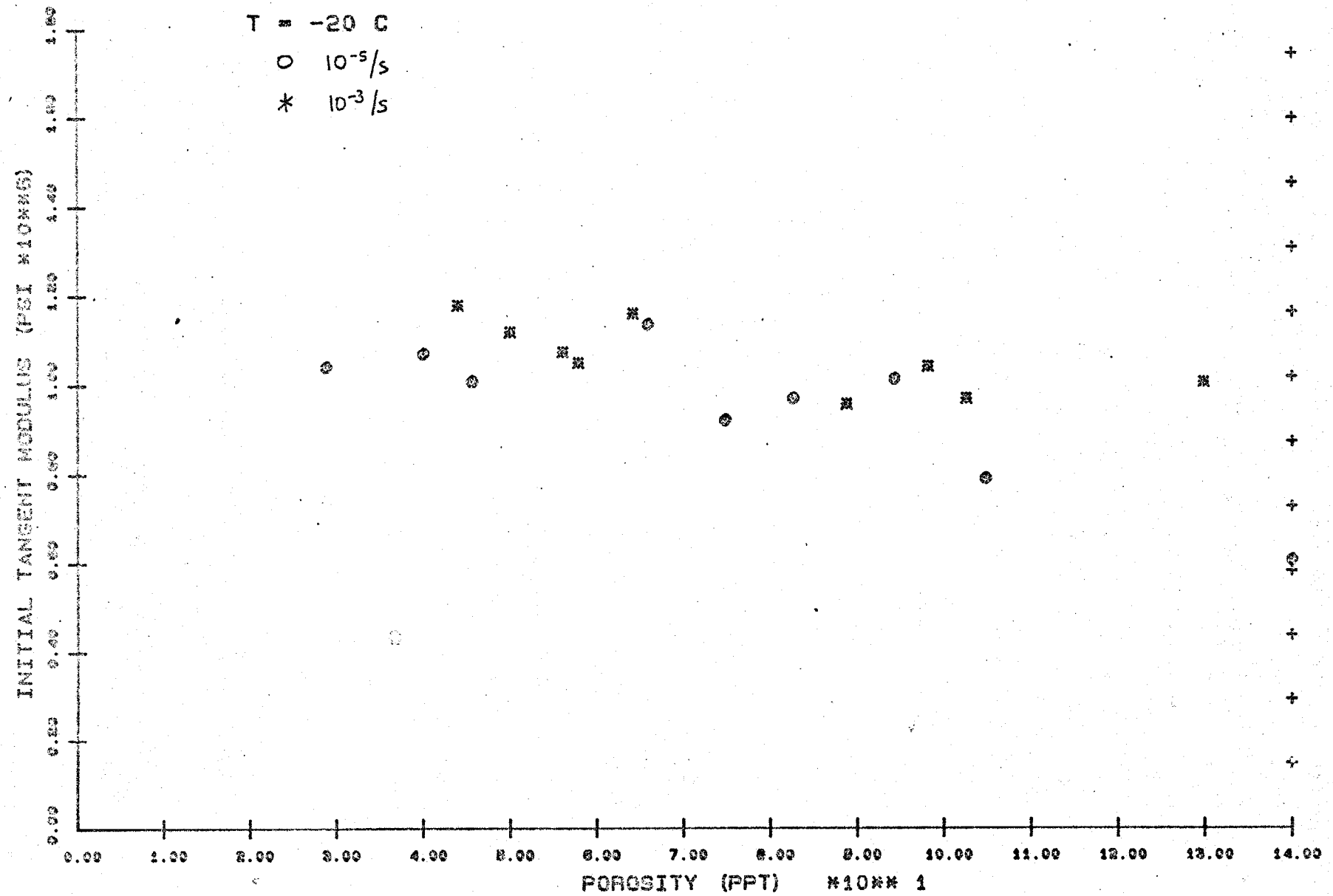
T = -20 C
O 10⁻⁵/s
* 10⁻³/s
INITIAL TANGENT MODULUS (PSI *10**6)
0.00
0.20
0.40
0.60
0.80
1.00
1.20
1.40
1.60
0.00
1.00
2.00
3.00
4.00
5.00
6.00
7.00
8.00
9.00
10.00
11.00
12.00
13.00
14.00
POROSITY (PPT) *10** 1

APPENDIX A

Constant Strain-Rate Compression Data

This appendix contains the results from the constant strain-rate, uniaxial compression tests (CSC). The parameters listed for each test are defined in the Index. CSC - 4-5 denotes those tests conducted at a strain-rate of 10^{-4}/s and a temperature of -5°C (23°F), etc.

INDEX

Column No.	Symbol	Description
1	σ_m, psi	Peak Stress
2	ε_m(GL),%	Strain at σ_m determined by the DCDT's over a guage length of 5.5 inches
3	ε_m(FS),%	Strain at σ_m determined by the extensometer over the full sample length of 10 inches
4	t_m, sec	Time to peak stress
5	σ_e, psi	Stress at end of test
6	ε_e(FS),%	Full sample strain at end of test
7	t_e, sec	Time to end of test
8	E_i(GL),x10^6psi	Initial tangent modulus determined using strains found over the gauge length
9	E_o(GL),x10^6psi	Secant modulus determined using gauge length strains
10	E_o(FS),x10^6psi	Secant modulus determined using full sample strains
11	S_i,$^o/_{oo}$	Sample salinity at test temperature
12	ρ, lb/ft^3	Sample density at test temperature
13	V_b,$^o/_{oo}$	Brine volume at test temperature
14	V_a,$^o/_{oo}$	Air volume at test temperature
15	n,$^o/_{oo}$	Porosity at test temperature
16	σ_e /σ_m	Ratio of end to peak stress
17	Ice squareness, in	Sample squareness after ends are milled
18	End cap squareness, in	Sample squareness after endcaps are mounted
19	Shim, in	Amount of shim stock inserted between low end of sample and actuator before testing
20	ν_o	Initial Poisson's Ratio; circumferential and gauge length strain measurements used
21	ν_m	Poisson's ratio at peak stress; ε_m(C) and ε_m(GL) used
22	ε_m(C),%	Strain at σ_m determined by the circumferential extensometer

Also Note: FILE B-3-5 indicates Below Level Ice

10^{-3}/sec Strain Rate

-5°C Test Temperature

FILE CSC-2-5

SAMPLE # 01	02	03	04	05	06	07	08	09	10	11	12	13	14	15	16	17	18	19	20	21	22
RA201-262/289	820	0.100	0.120	0.14	820	0.12	0.14	0.709	0.820	0.586	0.43	53.89	4.0	60.1	64.1		0.003	0.007	0.007	0.10	0.31	0.03
RA206-131/158	390	0.050	0.060	0.07	390	0.06	0.07	0.785	0.780	0.650	0.04	48.69	0.3	150.2	150.6		0.010	0.006	0.006	0.02	0.07	0.04
RA206-337/364	621	0.070	0.110	0.11	621	0.11	0.11	0.869	0.887	0.565	1.35	51.74	12.0	98.9	110.9		0.011	0.003	0.003	0.07	0.12	0.01
RC229-112/139	708	0.070	0.030	0.09	708	0.03	0.09	0.992	1.011	2.360	0.85	56.15	8.2	21.3	29.5		0.004	0.010	0.014	0.08	0.14	0.01
RC229-179/206	716	0.080	0.080	0.11	716	0.08	0.11	0.947	0.895	0.895	1.44	55.70	13.8	30.0	43.9		0.010	0.002	0.002	0.04	0.11	0.01
RC229-342/369	470	0.020	0.060	0.08	470	0.06	0.08	0.840	2.350	0.783	2.46	55.00	23.3	43.8	67.1		0.012	0.005	0.005	0.06	0.26	0.01
RC231-125/152	788	0.080	0.110	0.13	788	0.11	0.13	1.000	0.985	0.716	0.39	54.64	3.7	47.0	50.7		0.008	0.011	0.011	0.12	0.19	0.02
RC231-197/224	645	0.070	0.090	0.12	645	0.09	0.12	0.975	0.921	0.717	2.61	55.00	24.8	44.0	68.8		0.005	0.006	0.006	0.11	0.16	0.07
RC231-278/305	931	0.080	0.100	0.12	931	0.10	0.12	0.995	1.164	0.931	1.84	56.92	18.1	9.5	27.5		0.004	0.003	0.003	0.06	0.15	0.01

FILE CSC-4-5

SAMPLE # 01	02	03	04	05	06	07	08	09	10	11	12	13	14	15	16	17	18	19	20	21	22
R32-133/140V 330	0.150	0.170	16.50	195	5.00	500.0	0.771	0.220	0.194	1.17	53.50	10.8	68.0	78.8	0.591	0.003	0.006	0.006	0.08	0.34	0.05
R43-150H 386	0.110	0.110	10.60	223	5.00	500.0	0.739	0.351	0.351	0.48	51.62	4.3	99.7	104.0	0.578	0.048	0.010	0.010	0.05	0.10	0.01
R33-205/232V 478	0.100	0.090	7.80	207	5.00	500.0	0.983	0.478	0.531	3.05	55.18	29.0	41.6	70.6	0.433	0.007	0.005	0.005	0.04	0.31	0.03
R43-222H 402	0.260	0.270	25.40	203	5.00	500.0	0.671	0.155	0.149	1.82	54.98	17.3	43.1	60.4	0.505	0.090	0.012	0.012	0.02	0.77	0.20
R46-047/073V 362	0.090	0.080	7.10	131	5.00	500.0	0.807	0.402	0.453	0.92	54.24	8.6	54.6	63.3	0.362	0.009	0.003	0.003	0.09	0.08	0.01
R44-073H 326	0.090	0.040	5.90	123	5.00	500.0	0.921	0.362	0.815	1.28	53.13	11.7	74.5	86.2	0.377	0.027	0.016	0.016	0.06	0.16	0.01
R44-086H 227	0.110	0.110	11.70	91	5.00	500.0	0.639	0.206	0.206	1.23	50.69	10.8	116.9	127.7	0.403	0.033	0.000	0.004	0.19	0.40	0.04
R46-083/110V 800	0.620	0.400	37.70	247	5.00	500.0	1.068	0.129	0.200	2.62	55.12	24.9	41.8	66.7	0.309	0.006	0.005	0.005	0.13	0.13	0.08
R44-086H 390	0.110	0.090	5.80	95	5.00	500.0	0.999	0.355	0.433	1.85	57.03	18.2	7.6	25.8	0.245	0.035	0.009	0.009	0.05	0.12	0.01
R46-147/173V 271	0.150	0.120	14.00	115	5.00	500.0	0.846	0.181	0.226	2.99	55.19	28.5	41.2	69.7	0.424	0.006	0.003	0.003	0.13	0.33	0.05
R44-156H 175	0.060	0.090	5.50	139	5.00	500.0	0.834	0.292	0.194	2.64	55.89	25.5	28.5	54.0	0.794	0.013	0.004	0.004	0.14	0.23	0.01
R46-246/272V 446	0.090	0.110	9.30	191	5.00	500.0	1.006	0.496	0.406	3.29	54.99	31.2	45.3	76.5	0.428	0.008	0.009	0.006	0.05	0.05	0.01
R44-256H 271	0.080	0.080	6.60	111	5.00	500.0	0.818	0.339	0.339	2.62	55.74	25.2	31.2	56.4	0.410	0.033	0.015	0.013	0.03	0.09	0.01
R47-125/053V 322	0.100	0.090	9.00	127	5.00	500.0	0.782	0.322	0.358	1.05	53.25	9.6	72.2	81.8	0.394	0.005	0.011	0.011	0.06	0.11	0.01
R45-040H 306	0.060	0.080	6.30	111	5.00	500.0	0.671	0.510	0.383	0.30	49.32	2.6	139.6	142.2	0.363	0.045	0.041	0.041			
R47-191/217V 669	0.110	0.070	6.00	163	5.00	500.0	1.144	0.608	0.956	2.83	56.25	27.5	22.7	50.2	0.244	0.007	0.013	0.013	0.07	0.23	0.02
R44-204H 561	0.160	0.180	16.60	151	5.00	500.0	1.074	0.351	0.312	3.91	57.19	38.6	8.2	46.7	0.269	0.034	0.001	0.001	0.09	0.34	0.06
R47-275/302V 326	0.170	0.200	18.50	123	5.00	500.0	0.815	0.192	0.163	4.31	56.67	42.1	17.8	59.9	0.377	0.004	0.008	0.008	0.12	0.45	0.08
R44-288H 366	0.120	0.130	15.00	163	5.00	500.0	0.854	0.305	0.282	2.16	54.43	20.3	53.3	73.5	0.445	0.034	0.015	0.015	0.09	0.45	0.05

FILE CSC-2-20

SAMPLE # 01	02	03	04	05	06	07	08	09	10	11	12	13	14	15	16	17	18	19	20	21	22
RA201-009/036																					
597	0.080	0.100	0.12	597	0.10	0.12	0.765	0.746	0.597	0.01	46.95	0.0	182.4	182.4		0.003	0.003	0.003	0.18	0.29	0.02
RA201-078/105																					
1130	0.130	0.140	0.16	1130	0.14	0.16	0.887	0.869	0.807	0.02	50.14	0.1	126.9	126.9		0.006	0.004	0.004	0.26	0.29	0.04
RA201-339/366																					
1361	0.130	0.140	0.16	1361	0.14	0.16	1.068	1.047	0.972	0.63	55.42	2.0	35.5	37.5		0.004	0.003	0.003	0.22	0.34	0.04
RA201-428/455																					
1476	0.160	0.160	0.17	1476	0.16	0.17	1.024	0.923	0.923	0.98	55.68	3.2	31.3	34.5		0.037	0.010	0.010	0.24	0.41	0.06
RA206-058/085																					
971	0.090	0.120	0.13	971	0.12	0.13	1.522	1.079	0.809	0.02	52.04	0.1	93.8	93.8		0.007	0.017	0.017	0.20	0.32	0.03
RA206-266/293																					
1154	0.130	0.120	0.15	1194	0.12	0.15	0.882	0.919	0.995	0.24	50.51	0.7	120.6	121.3		0.008	0.003	0.003	0.24	0.30	0.04
RC229-251/278																					
1448	0.130	0.120	0.16	1448	0.12	0.16	1.232	1.114	1.207	2.58	56.51	8.5	18.5	27.0		0.006	0.004	0.004	0.17	0.28	0.04
RC231-350/377																					
1058	0.090	0.090	0.13	1058	0.09	0.13	1.156	1.176	1.176	2.14	56.19	7.0	23.6	30.6		0.006	0.007	0.007	0.21	0.30	0.03
RC231-416/443																					
1520	0.120	0.160	0.18	1520	0.16	0.18	1.255	1.267	0.950	1.83	57.07	6.1	8.0	14.1		0.004	0.001	0.001	0.22	0.44	0.05

FILE CSC-4-20

SAMPLE # 01	02	03	04	05	06	07	08	09	10	11	12	13	14	15	16	17	18	19	20	21	22
R32-231/258V 963	0.210	0.280	22.50	485	5.00	500.0	1.233	0.459	0.344	3.76	55.68	12.2	34.0	46.2	0.504	0.002	0.000	0.000	0.21	0.50	0.10
R43-245H 546	0.080	0.100	9.50	167	5.00	500.0	1.159	0.683	0.546	3.07	56.46	10.1	19.8	29.9	0.306	0.042	0.012	0.009	0.25	0.48	0.04
R32-267/294V 661	0.140	0.220	21.10	167	5.00	500.0	1.036	0.472	0.301	3.76	55.92	12.3	22.9	42.1	0.253	0.012	0.010	0.010			
R33-268/295V 899	0.140	0.170	13.50	334	1.40	13.50	1.278	0.642	0.529	4.35	57.13	14.5	9.4	24.0		0.010	0.001	0.001	0.16	0.38	0.05
R43-280H 708	0.110	0.100	9.70	143	5.00	500.0	1.490	0.644	0.708	3.39	56.04	11.1	27.4	38.5	0.202	0.033	0.006	0.006	0.09	0.44	0.05
R32-303/328V 573	0.130	0.110	11.70	223	5.00	500.0	0.878	0.441	0.521	1.48	54.09	4.7	59.4	64.1	0.389	0.010	0.005	0.005	0.15	0.59	0.08
R43-316H 342	0.070	0.090	8.20	231	5.00	500.0	1.191	0.489	0.380	3.71	56.63	12.3	17.5	29.8	0.675	0.025	0.027	0.027	0.09	0.32	0.02
R32-343/369V 485	0.170	0.240	23.90	175	5.00	500.0	0.776	0.285	0.202	2.51	52.92	7.8	80.7	88.5	0.361	0.006	0.015	0.015	0.21	0.47	0.08
R43-357H 597	0.140	0.130	14.40	239	5.00	500.0	0.965	0.426	0.459	1.67	54.45	5.3	53.4	58.7	0.400	0.038	0.006	0.006	0.19	0.42	0.06
R33-242/268V 947	0.190	0.190	19.40	700	0.59	61.00	1.287	0.498	0.498	5.91	56.94	16.7	13.4	30.1		0.005	0.005	0.005	0.17	0.31	0.06
R43-257H 541	0.100	0.100	11.00	215	5.00	500.0	1.144	0.541	0.541	3.61	56.92	12.0	12.4	24.4	0.397			0.008	0.18	0.52	0.05
R33-368/395V 939	0.180	0.160	14.20	247	5.00	500.0	1.101	0.522	0.587	4.52	56.20	14.8	25.7	40.6	0.263	0.006	0.004	0.004	0.17	0.70	0.12
R43-381H 867	0.130	0.150	14.30	207	5.00	500.0	1.179	0.667	0.578	0.44	55.74	1.3	29.7	31.0	0.239	0.025	0.003	0.003	0.26	0.59	0.08
R46-121/147V 517	0.100	0.100	10.50	163	5.00	500.0	1.101	0.517	0.517	2.58	53.89	8.1	64.0	72.1	0.315	0.012	0.006	0.006	0.14	0.43	0.04
R44-128H 255	0.080	0.090	9.50	151	5.00	500.0	0.952	0.319	0.283	3.27	56.60	10.8	17.6	28.4	0.592	0.037	0.009	0.009	0.23	0.37	0.03
R46-173/199V 493	0.110	0.120	12.10	175	5.00	500.0	0.873	0.448	0.411	1.70	53.77	5.3	65.1	70.4	0.355	0.009	0.008	0.008	0.23	0.40	0.04
R44-186H 1018	0.130	0.110	12.40	302	5.00	500.0	1.292	0.783	0.926	3.68	56.51	12.1	19.4	31.6	0.297	0.024	0.006	0.006	0.16	0.23	0.03
R46-276/303V 629	0.120	0.120	13.40	223	5.00	500.0	0.952	0.524	0.524	1.02	53.72	3.2	65.5	68.7	0.355	0.006	0.005	0.005	0.21	0.59	0.05
R44-299H 609	0.120	0.120	13.50	269	5.00	500.0	0.900	0.508	0.508	1.60	54.99	5.1	43.8	48.9	0.442	0.058	0.013	0.013	0.17	0.38	0.05
R47-090/116V 1798	0.190	0.210	20.70	1397	0.27	25.70	1.311	0.946	0.856	3.49	55.92	11.4	29.6	41.0		0.026	0.002	0.002	0.19	0.42	0.08
R44-103H 505	0.100	0.080	7.30	195	5.00	500.0	1.111	0.505	0.631	3.09	56.16	10.1	24.7	34.8	0.386	0.032	0.006	0.006			
R44-116H 243	0.070	0.070	6.60	111	5.00	500.0	0.921	0.347	0.347	3.71	56.79	11.0	14.3	25.3	0.457	0.010	0.005	0.005	0.21	0.47	0.04
R47-127/153V 1846	0.180	0.120	14.60	1846	0.10	14.60	1.406	1.026	1.538	3.28	56.16	10.8	25.2	36.0		0.011	0.004	0.004	0.14	0.34	0.06
R44-141H 287	0.080	0.110	9.30	195	5.00	500.0	1.096	0.359	0.261	3.54	57.35	11.9	4.7	16.6	0.470	0.040	0.003	0.003	0.23	0.32	0.02
R47-302/329V 875	0.110	0.130	10.00	247	5.00	500.0	1.352	0.796	0.875	2.57	56.71	8.5	15.0	23.5	0.282	0.005	0.009	0.009	0.18	0.30	0.03

APPENDIX B

Constant Strain-Rate Compression Data

This appendix contains the results from the constant strain-rate, uniaxial tension tests (CST). The parameters listed for each tests are defined in the Index.

FILE CST-5-5

SAMPLE # 01	02	03	04	05	06	07	08	09	10	11	12	13	14	15	16	17	18	19	20	21	22
RA207-181/208	135	0.018	0.022	21.80			0.913	0.750	0.614	0.05	52.87	0.5	77.2	77.6		0.006	0.007				
RA209-036/063	149	0.022	0.026	21.20			1.100	0.677	0.573	0.03	50.85	0.3	112.3	112.6		0.006	0.009				
RA209-291/318	138	0.019	0.029	28.60			1.020	0.726	0.476	0.76	56.36	7.4	17.3	24.7		0.006	0.004				
RB220-129/156	94	0.014	0.014	14.00			0.990	0.676	0.676	0.54	53.25	8.6	71.9	80.5		0.006	0.000				
RB221-164/191	113	0.020	0.020	19.80			0.889	0.565	0.565	1.63	54.64	15.4	48.8	64.2		0.005	0.006				
RB221-196/223	82	0.019	0.032	32.30			0.887	0.432	0.257	1.99	55.31	19.0	37.5	56.5		0.007	0.009				
RB221-257/284	136	0.019	0.026	25.30			0.817	0.716	0.523	1.12	53.96	10.4	59.8	70.2		0.005	0.009				
RB222-018/045	94	0.021	0.025	24.90			0.786	0.451	0.378	0.02	49.33	0.2	138.9	139.1		0.010	0.005				
RB222-163/190	130	0.018	0.017	17.00			0.940	0.722	0.765	0.91	53.37	8.4	69.8	78.1		0.005	0.003				

FILE CST-3-5

SAMPLE #	01	02	03	04	05	06	07	08	09	10	11	12	13	14	15	16	17	18	19	20	21	22
RA203-073/100	115	0.013	0.015	0.32				0.812	0.885	0.767	0.01	51.12	0.1	107.6	107.7		0.006	0.001				
RA207-149/176	116	0.011	0.012	0.33				1.124	1.055	0.967	0.04	52.53	0.4	83.1	83.4		0.015	0.005				
RA207-263/290	71	0.008	0.009	0.26				0.943	0.891	0.792	0.57	52.94	5.2	76.7	81.9		0.006	0.004				
RB214-232/259	76	0.006	0.009	0.26				0.945	0.950	0.844	3.43	53.13	31.4	77.7	109.2		0.049	0.012				
RB214-263/290	120	0.012	0.014	0.33				1.054	1.000	0.857	1.38	54.67	13.0	47.9	60.9		0.009	0.000				
RB220-039/066	60	0.007	0.008	0.23				0.977	0.863	0.755	0.21	50.60	1.8	116.9	118.8		0.006	0.006				
RB220-161/188	91	0.009	0.009	0.27				0.931	1.017	1.017	0.38	53.77	3.5	62.0	65.5		0.010	0.003				
RB220-193/220	84	0.007	0.010	0.25				1.207	1.203	0.842	2.20	55.42	21.0	36.0	57.0		0.004	0.014				
RB221-005/032	69	0.011	0.012	0.27				0.616	0.633	0.580	0.02	40.80	0.1	287.9	288.0		0.026	0.018				

FILE CST-5-20

SAMPLE # 01	02	03	04	05	06	07	08	09	10	11	12	13	14	15	16	17	18	19	20	21	22
RA203-192/219	93	0.010	0.010	9.80			1.134	0.935	0.935	0.03	53.64	0.1	65.8	65.9		0.006	0.005				
RA203-243/270	123	0.014	0.014	14.10			1.011	0.879	0.879	0.51	52.12	1.6	92.7	94.3		0.005	0.001				
RA203-341/368	126	0.014	0.016	15.50			1.069	0.900	0.788	1.41	55.46	4.6	35.4	40.0		0.007	0.002				
RA207-005/032	78	0.014	0.015	14.60			0.604	0.557	0.520	0.01	45.93	0.0	200.1	200.1		0.003	0.010				
RA209-129/156	92	0.011	0.012	12.10			0.967	0.841	0.771	0.08	52.69	0.2	82.4	82.6		0.011	0.007				
RA209-160/187	89	0.012	0.012	12.30			0.788	0.745	0.745	0.01	51.40	0.0	104.8	104.8		0.003	0.003				
RB214-185/212	71	0.009	0.011	10.60			0.919	0.793	0.649	0.47	53.23	1.5	73.3	74.8		0.005	0.003				
RB214-363/395	134	0.022	0.025	24.50			1.039	0.609	0.536	3.16	56.84	10.4	18.4	28.8		0.016	0.007				
RB220-231/258	124	0.012	0.018	15.80			1.006	1.033	0.689	0.97	55.03	3.1	42.5	45.6		0.005	0.008				